A STUDY ON THE IMPORTANCE OF AN INTACT-RING STRUCTURE IN PROLINE RACEMASE CATALYSIS

by

Pooja Srinivasan

Submitted in partial fulfilment of the requirements
for the degree of Master of Science

at

Dalhousie University
Halifax, Nova Scotia
August 2018

© Copyright by Pooja Srinivasan, 2018

TABLE OF CONTENTS

LIST OF TABLES ..... **v**
LIST OF FIGURES ..... **vi**
LIST OF SCHEMES ..... **viii**
ABSTRACT ..... **ix**
LIST OF ABBREVIATIONS USED ..... **x**
ACKNOWLEDGEMENTS ..... **xii**
CHAPTER 1 INTRODUCTION **1**
1.1 PROLINE RACEMASE (PR) 1
1.1.1 Proline racemase family 1
1.1.2 Expression and characterisation of proline racemase 5
1.1.3 The structure of proline racemase 7
1.1.4 Mechanism of PR catalysis 10
1.1.5 Substrates and inhibitors of PR 11
1.2 TEMPERATURE-DEPENDENCE OF ENZYME CATALYSIS 13
1.3 THERMODYNAMICS OF ENZYME CATALYSIS 16
1.3.1 Transition state stabilisation 16
1.3.2 The role of entropy in enzyme catalysis 19
1.4 THESIS OVERVIEW 21
CHAPTER 2 KINETICS AND ENERGETICS OF THERMOPHILIC AND MESOPHILIC VARIANTS OF PROLINE RACEMASE: A COMPARATIVE STUDY **23**
2.1 INTRODUCTION 23
2.2 MATERIALS AND METHODS 24
2.2.1 General 24
2.2.2 Production and purification of *Cs*PR 25
2.2.3 Cloning of *Tl*PR 26
2.2.4 Production and purification of *Tl*PR 26
2.2.5 Circular dichroism spectroscopy-based PR assays for temperature-dependence studies 27

2.2.6 Data analysis 28
2.3 RESULTS 30
2.3.1 Eyring-Polanyi and van't Hoff plots for *Cs*PR catalysis 30
2.3.2 Eyring-Polanyi and van't Hoff plots for *Tl*PR catalysis 30
2.3.3 Free energy profiles for *Cs*PR and *Tl*PR catalysed racemisation of L- and D-proline 34
2.4 DISCUSSION 34

CHAPTER 3 INHIBITION AND KINETICS OF CsPR WITH THE SUBSTRATE ANALOGUE, *N*-ETHYL-L-ALANINE 45

3.1 INTRODUCTION 45
3.2 MATERIALS AND METHODS 46
3.2.1 General 46
3.2.2 Synthesis of *N*-ethyl-L-alanine 48
3.2.3 Molar ellipticity of *N*-ethyl-L-alanine 49
3.2.4 Circular dichroism spectroscopy-based *Cs*PR assay of L-NEA binding 49
3.2.5 Circular dichroism spectroscopy-based *Cs*PR assay with *N*-ethyl-L-alanine as the substrate 50
3.2.6 *Cs*PR assay using HPLC-OR detection 50
3.2.7 Data analysis 51
3.3 RESULTS 52
3.3.1 Product analysis 52
3.3.2 Inhibition of *Cs*PR by *N*-ethyl-L-alanine 52
3.3.3 *N*-Ethyl-L-alanine as a substrate of *Cs*PR 59
3.4 DISCUSSION 59

CHAPTER 4 INVESTIGATION OF STERIC EFFECTS ON SUBSTRATE BINDING DURING PROLINE RACEMASE CATALYSIS 64

4.1 INTRODUCTION 64
4.2 MATERIALS AND METHODS 65
4.2.1 General 65
4.2.2 Molar ellipticity of L- and D-pipecolic acid 66
4.2.3 Circular dichroism spectroscopy-based *Cs*PR assay with L- and D-pipecolic acid 66

4.2.4 Molar ellipticity of *N*-methyl-L-alanine and *N*-methyl-D-alanine 66
4.2.5 Inhibition of *Cs*PR catalysis by *N*-methyl-L-alanine 67
4.2.6 Circular dichroism spectroscopy-based *Cs*PR assay with *N*-methyl-L-alanine and *N*-methyl-D-alanine 67
4.2.7 Molar ellipticity of L-azetidine-2-carboxylic acid 68
4.2.8 Circular dichroism spectroscopy-based PR assay with L-azetedine-2-carboxylic acid 68
4.2.9 Data analysis 68
4.3 RESULTS 69
4.3.1 Pipecolic acid as a substrate of *Cs*PR 69
4.3.2 *N*-Methylalanine as a substrate of *Cs*PR 72
4.3.3 *N*-Methylalanine as an inhibitor of *Cs*PR 72
4.3.4 L-Azetidine-2-carboxylic acid as a substrate of *Cs*PR 76
4.4 DISCUSSION 76
CHAPTER 5 CONCLUSIONS 88
REFERENCES 91

LIST OF TABLES

Table 1.1 List of inhibitors of proline racemase catalysis 14

Table 2.1 Kinetic parameters for the *Cs*PR-catalysed racemisation of (a) L-proline and (b) D-proline by *Cs*PR at different temperatures..... 31

Table 2.2 Kinetic parameters for the *Cs*PR-catalysed racemisation of (a) L-proline and (b) D-proline by *Tl*PR at different temperatures..... 35

Table 2.3 Change in enthalpy ($\Delta H^{\ddagger}$), entropy ($\Delta S^{\ddagger}$), and Gibbs free energy ($\Delta G^{\ddagger}$) of activation and the enthalpy (ΔH_s), entropy (ΔS_s), free energy (ΔG_s) of substrate binding of *Cs*PR and *Tl*PR catalysis. 39

Table 4.1 Summary of the catalytic efficiencies (k_{cat}/K_m) and free energies of activation ($\Delta G^{\ddagger}$) for the racemisation of various substrates catalysed by *Cs*PR..... 80

Table 4.2 Entropies of the substrates as zwitterions in water at 15 °C obtained by DFT-QM calculations at 631-G* level. 87

LIST OF FIGURES

Figure 1.1 Metabolic pathway of L- and D-proline in *Trypanosoma cruzi*. 6

Figure 1.2 Active site of proline racemase from *T. cruzi* with pyrrole-2-carboxylic acid bound. 8

Figure 1.3 Free energy profile for enzymatic and non-enzymatic conversion of substrate to product. 20

Figure 2.1 Images of SDS-PAGE gels (12%) 29

Figure 2.2 Temperature dependence of the kinetic parameters for the *Cs*PR-catalysed racemisation of L-proline. 32

Figure 2.3 Temperature dependence of the kinetic parameters for the *Cs*PR-catalysed racemisation of D-proline. 33

Figure 2.4 Temperature dependence of the kinetic parameters for the *Tl*PR-catalysed racemisation of L-proline. 36

Figure 2.5 Temperature dependence of the kinetic parameters for the *Tl*PR-catalysed racemisation of D-proline. 37

Figure 2.6 Reaction coordinate diagram for reactions catalysed by *Cs*PR and *Tl*PR with L- and D-proline as substrates. 38

Figure 2.7 Logarithmic scale of enzymatic (k_{cat}) and non-enzymatic (k_{non}) rate constants for some representative reactions. 43

Figure 2.8 Logarithmic scale of enzyme efficiencies (k_{cat}/K_m) and non-enzymatic (k_{non}) rate constants for some representative reactions 44

Figure 3.1 Substrates and inhibitors of *Cs*PR catalysis. 47

Figure 3.2 ^{1}H NMR spectrum of *N*-ethyl-L-alanine in D_2O. 53

Figure 3.3 ^{13}C NMR spectrum of *N*-ethyl-L-alanine in D_2O. 54

Figure 3.4 Mass spectra of *N*-ethyl-L-alanine. 55

Figure 3.5 Circular dichroism spectrum of L-NEA. 56

Figure 3.6 Standard curve of L-NEA to determine its molar ellipticity. 57

Figure 3.7 IC_{50} curves for the inhibition of *Cs*PR-catalysed racemisation of L-proline by L-NEA at 37 °C (A) and 15 °C (B). 58

Figure 3.8 Change in ellipticity of L-NEA in a *Cs*PR-catalysed reaction. 60

Figure 3.9 HPLC-OR assay for analysing L-NEA turnover in the reaction catalysed by *Cs*PR. 61

Figure 4.1 Standard curve for determination of the molar ellipticities of L- and D-pipecolic acid. 70

Figure 4.2 Representative Michaelis-Menten plots for *Cs*PR-catalysed racemisation of (A) L-pipecolic acid and (B) D-pipecolic acid. 71

Figure 4.3 Standard curve of L-NMA to determine its molar ellipticity..... 73

Figure 4.4 Representative Michaelis-Menten plots for *Cs*PR-catalysed racemisation of (A) L-NMA and (B) D-NMA. 74

Figure 4.5 Representative IC_{50} curve of *Cs*PR catalysis with L-NMA as the inhibitor. 75

Figure 4.6 Inhibition kinetics of *Cs*PR by L-NMA. 77

Figure 4.7 Standard curve for the determination of the molar ellipticity of L-ACA. 78

Figure 4.8 Representative Michaelis-Menten plot for *Cs*PR-catalysed racemisation of L-ACA. 79

Figure 4.9 A comparison between free energies of activation ($\Delta G^{\ddagger}$) and the catalytic efficiencies (k_{cat}/K_m) of *Cs*PR-catalysed racemisation of L-ACA and L-NMA. 86

LIST OF SCHEMES

Scheme 1.1 Reaction catalysed by proline racemase 2

Scheme 1.2 Reaction catalysed by hydroxyproline epimerase 3

Scheme 1.3 Reaction catalysed by *trans*-l,3-hydroxyproline dehydratase (transHypD) 4

Scheme 1.4 Two-base mechanism of proline racemase-catalysed reaction 12

Scheme 1.5 Thermodynamic cycle representing the equilibria between the enzymatic and non-enzymatic reactions 17

Scheme 4.1 Reaction mechanism for linear-mixed mode of inhibition of *Cs*PR (E)-catalysed racemisation of L-proline (S) by L-NMA (I) 83

ABSTRACT

Proline racemase (PR) catalyses the interconversion of L-proline and D-proline, in a cofactor-independent manner. PR follows a two-base mechanism, using two Cys residues in the active site that act as enantiospecific Brønsted bases, to catalyse the interconversion of the stereoisomers of proline via an *aci*-carboxylate intermediate.

A kinetic study was conducted between the mesophilic PR from *Clostridium sticklandii* (*Cs*PR) and a hyperthermophilic PR from *Thermococcus litoralis* (*Tl*PR) based on their thermodynamic contributions to proline racemisation. Free energy profiles of both *Cs*PR and *Tl*PR suggested that they follow similar energy paths during catalysis, but *Cs*PR showed slightly greater binding affinity with proline than *Tl*PR.

A kinetic analysis of the open-ring proline analogue, *N*-ethyl-L-alanine (NEA) revealed a dramatic decrease of ~4,500-fold in catalytic efficiency of *Cs*PR-catalysed racemisation of L-NEA relative to that of L-proline. To study the importance of steric factors on *Cs*PR catalysis, a variety of other proline analogues, including pipecolic acid, L-azetedine-2-carboxylic acid and *N*-methylalanine (NMA) were examined for their ability to act as substrates of *Cs*PR. *Cs*PR catalysed the racemisation of all three compounds, but with markedly reduced catalytic efficiencies relative to proline as a substrate. A rather surprising observation was that L-NMA acts both as a substrate and an inhibitor of *Cs*PR catalysis, following a linear-mixed mode of inhibition. The results presented in this thesis suggest that, both sterics and entropic effects contribute to *Cs*PR catalysis and the presence of an intact-ring in the substrate is crucial to activity.

LIST OF ABBREVIATIONS USED

ACA	L-azetidine-2-carboxylic acid
AspR	aspartate racemase
CBZ	carboxybenzyl
CD	circular dichroism
*Cs*PR	proline racemase from *Clostridium sticklandii*
DAPE	diaminopimelate epimerase
EC	enzyme commission number
EDTA	ethylenediaminetetraacetic acid
ES	enzyme-substrate complex
ESI	electrospray ionization
GAPDH	glyceraldehyde-3-phosphate dehydrogenase
GluR	glutamate racemase
HPLC	high-performance liquid chromatography
HypE	4-hydroxyproline epimerase
IPTG	isopropyl β-D-1-thiogalactopyranoside
LB	lysogeny broth media
MS	mass spectrometry
NEA	*N*-ethyl-L-alanine
NMA	*N*-methyl-L-alanine
NMR	nuclear magnetic resonance
OR	optical rotation
ORF	open reading frame
PAGE	polyacrylamide gel electrophoresis
PLP	pyridoxal phosphate
PR	proline racemase
PYC	pyrrole-2-carboxylic acid
SDS	sodium dodecyl sulfate
SPE	solid phase extraction
*Tc*ProR	proline racemase from *Trypanosoma cruzi*

THF	tetrahydrofuran
*Tl*PR	proline racemase from *Thermococcus litoralis*
TOF	time of flight
*trans*HypD	*trans*-L-3-hydroxyproline dehydratase
TS	transition state

ACKNOWLEDGEMENTS

I extend my sincere gratitude and thanks to Dr. Stephen L. Bearne for not only supervising me throughout my Masters, but also mentoring and shaping me during this journey. I am greatly inspired by his dedication and passion for research. I am very fortunate to have this opportunity to learn from this excellent teacher who patiently guided me and always pushed me to work harder to become a better researcher.

I would like to thank my committee members, Dr. Jan Rainey and Dr. Catherine Too for their valuable feedback and critical advice that was extremely important for my progress. I would also like to thank Dr. David Langelaan and Dr. Vanya Ewart for taking time to reviewing my thesis. I thank Dr. Bearne and the funding agencies, Natural Sciences and Engineering Council (NSERC) and Nova Scotia Health Research Foundation (NSHRF) for funding me during the two years of my thesis work. I sincerely thank the Department of Biochemistry and Molecular biology and Faculty of Graduate studies, Dalhousie University for considering my candidature and awarding me with the One-year Nova Scotia Graduate Scholarship.

Talking about the Department of Biochemistry and Molecular biology, I extend my special thanks to Roisin for being so supportive and caring, for being the kind person she is and we will always share a special bond. I am also thankful to Barb and Brenda for their continued support in administrative matters.

I would like to thank members of the Bearne lab: Greg, Sarah, Colin, Himank, Einat, Amar, Chris, Nicole and Minglu for all their insightful discussions, support and for the fun I had whilst working with them in the lab. Special thanks to Greg for helping me troubleshoot my cloning experiments.

I thank my parents, Srinivasan and Sheela, for being my support system and for always being there for me, even when I was oceans away from home. I also thank my little brother, Pranav, whose hilarious insanity has helped me stay sane. I thank my friends, Dhivya, Ruhi, Jeyabalaji and Yamani for being my family away from home. I thank my friends back in India, Aathira and Roshni, without whom this journey would have been impossible. Finally, I thank everyone, those mentioned and unmentioned above, for making this journey possible and delightful.

CHAPTER 1

INTRODUCTION

1.1 Proline Racemase (PR)

1.1.1 Proline racemase family

The proline racemase family broadly encompasses enzymes that catalyse racemisation and epimerisation reactions of proline and hydroxyproline, respectively. This includes proline racemase (EC:5.1.1.4) (Stadtman and Elliot, 1957), 4-hydroxyproline epimerase (EC:5.1.1.8) (Adams & Norton, 1964) and *trans*-L-3-hydroxyproline dehydratase (EC:4.2.1.77) (Visser, Verhoeven-duif, & Koning, 2012). Proline racemase (PR) catalyses the interconversion of L- and D-proline (**Scheme 1.1**), whereas 4-hydroxyproline epimerase (HypE) catalyses the epimerisation of 4-hydroxy-L-proline and 4-hydroxy-D-proline (**Scheme 1.2**) and *trans*-L-3-hydroxyproline dehydratase (*trans*HypD) catalyses the conversion of *trans*-L-3-hydroxyproline to 1-pyrroline-2-carboxylate (**Scheme 1.3**). The gene sequences encoding enzymes across the family are highly conserved, but the high substrate specificity arises from the differences in the active site architecture of each enzyme.

PR belongs to the subfamily of pyridoxal phosphate (PLP)-independent enzymes accompanied by glutamate racemase (GluR), aspartate racemase (AspR) and diaminopimelate epimerase (DAPE), as opposed to enzymes that depend on PLP as a cofactor for catalysis (e.g., alanine racemase, serine racemase, isoleucine epimerase, arginine racemase, among others) (Conti *et al*., 2011). The role of PLP in these enzymes is to increase the acidity of the C_{α}-hydrogen of their corresponding substrates (Rubinstein & Major, 2009). The increase in acidity arises, in part, from the

Scheme 1.1 Reaction catalysed by proline racemase

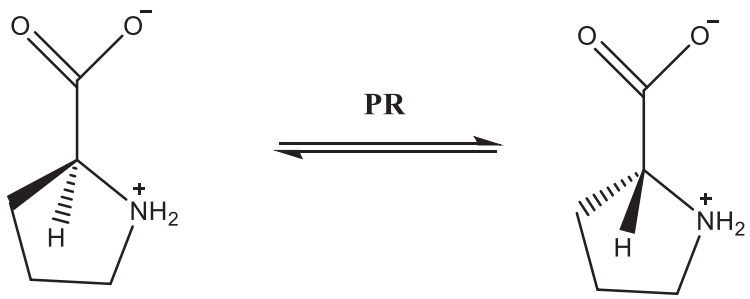

L-proline **D-proline**

Scheme 1.2 Reaction catalysed by hydroxyproline epimerase

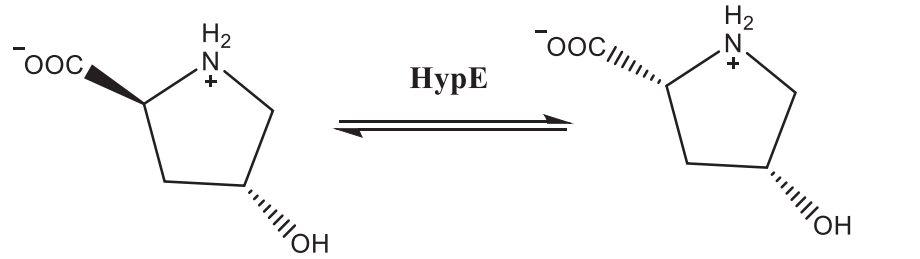

***trans*-4-hydroxy-L-proline** **HypE** ***cis*-4-hydroxy-D-proline**

Scheme 1.3 Reaction catalysed by *trans*-l,3-hydroxyproline dehydratase (*trans*HypD)

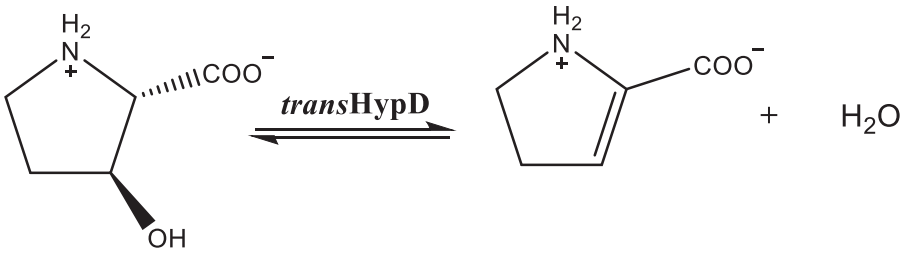

***trans*-1,3-hydroxy-L-proline** **1-pyrroline-2-carboxylate**

formation of a Schiff-base with the substrate leading to an aldimine, which has a decreased pK_a of the C_α-hydrogen from ~29 to pK_a values of 6 to 17 (as observed with a range of substrates), facilitating the removal of the C_α-hydrogen by an enzymatic Brønsted base during catalysis (Richard *et. al*., 2009). The PLP-independent racemases share a common mechanism of catalysis, i.e., a two-base mechanism involving a Cys dyad in the active site (Pillai *et al*., 2006).

1.1.2 Expression and characterisation of proline racemase

Proline racemase (PR) was first partially purified by Stadtman & Elliot, 1957 from the bacterium *Clostridium sticklandii.* Over a decade later, a pure preparation of the enzyme was obtained from *C. sticklandii* (*Cs*PR) by Cardinale & Abeles, 1968. The enzyme was unique among racemases due to its ability to catalyse the racemisation of L- and D-proline without the requirement of a cofactor (Cardinale & Abeles, 1968), similar to hydroxyproline epimerase, which also did not require a cofactor (Adams & Norton, 1964). PR was then shown to be expressed in various other prokaryotes for the metabolism of proline (**Figure 1.1**). The first eukaryotic PR was identified from the parasite *Trypanosoma cruzi* (*Tc*ProR, Reina-San-Martin *et al*., 2000). Reina-San-Martin *et al.* (2000) discovered the mitogenic properties of *Tc*ProR by identifying a 45 kDa mitogen encoded by two homologous genes, *Tc*45-A and *Tc*45-B, of which *Tc*45A exhibited high sequence homology with *Cs*PR (Reina-San-Martin *et al*., 2000). This protein was identified as a B-cell mitogen in *Trypanosoma* species, and a decrease in its mitogenic activity was observed in the presence of the PR inhibitor, pyrrole-2-carboxylic acid (Reina-San-Martin *et al*., 2000). This suggests that the PR protein has an epitope that promotes mitogenesis, but only in the

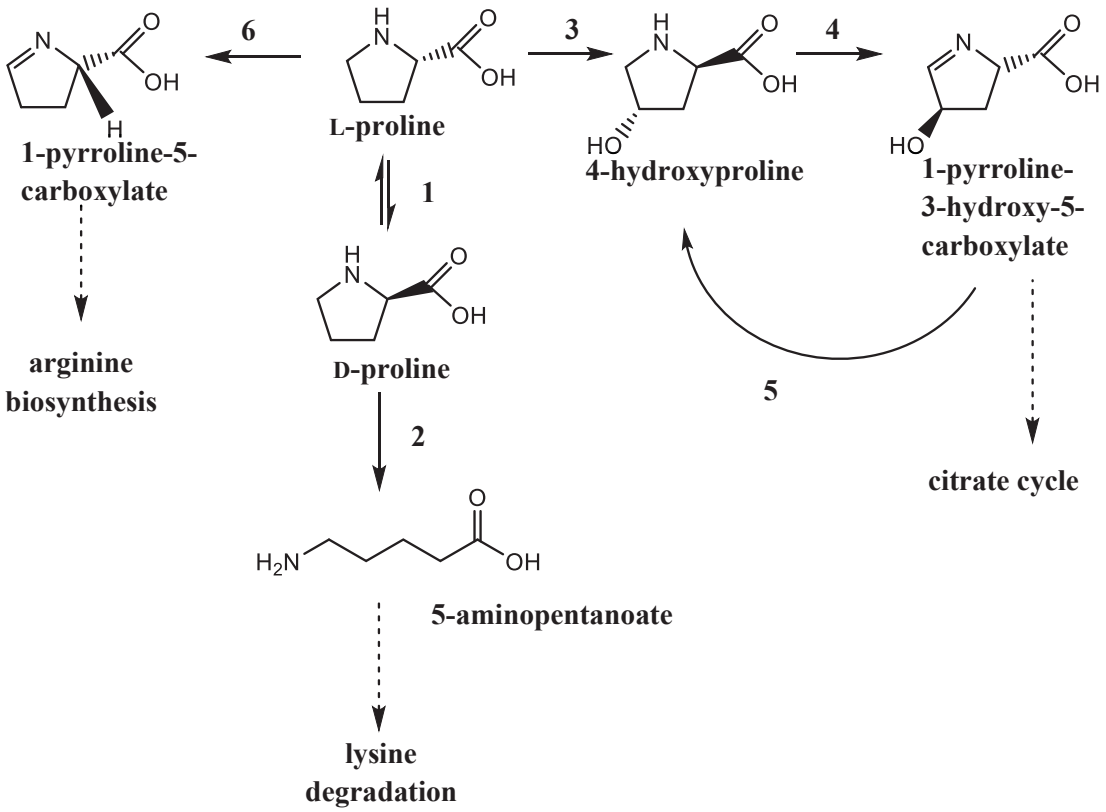

Figure 1.1 Metabolic pathway of L- and D-proline in *Trypanosoma cruzi*. The enzymes involved in this pathway are proline racemase (1), prolyl-4-hydroxylase (3), hydroxyproline dehydrogenase (4), pyrroline-5-carboxylate reductase (5) and proline dehydrogenase (6) (Kurihara *et. al.,* 2006; Kurihara *et. al.*, 2005).

ligand-free state (Reina-San-Martin *et al*., 2000). Thus, designing inhibitors against PR is key to developing strategies of treatment against diseases caused by this protozoan parasite, including Chagas disease (Reina-San-Martin *et al*., 2000).

Recently, a PR-like enzyme (*Tl*PR) was isolated from a hyperthermophillic archaeon, *Thermococcus litoralis*, with optimal growth temperatures between 50 and 100 °C (Watanabe *et al.*, 2015). *Tl*PR has a sequence homology of ~85% with the other enzymes of the PR family with a conserved active site architecture. In the current study, temperature dependent studies are conducted with the mesophilic (*Cs*PR) and the thermophilic (*Tl*PR) variants of PR.

1.1.3 The structure of PR

PR from *C. sticklandii* exists as a dimer in solution. Initially, Scatchard plot analysis with pyrrole-2-carboxylic acid (PYC) as the ligand revealed one ligand-binding site per dimer (Rudnick & Abeles 1975). However, this conclusion was disproven when the 2.1-Å resolution crystal structure of *T. cruzi* PR (*Tc*ProR) was solved with PYC bound. In the structure, each protomer of the homodimer was bound to one molecule of PYC (PDB 1W62) (Buschiazzo *et al.*, 2006). Each protomer consists of two structurally equivalent α/β domains and each domain is made up of three antiparallel three-stranded β-sheets and two α-helices (**Figure 1.2**). An extra N-terminal α-helix is observed in the ligand-free form of the enzyme obtained at low concentrations of PYC. The dimeric form of the protein has two interdomain interactions that hold the protomers together and a 20-Å deep crevice extends from the interdomain space into the protein towards the active site, allowing for entry of the substrate into the active site (Buschiazzo *et al.*, 2006).

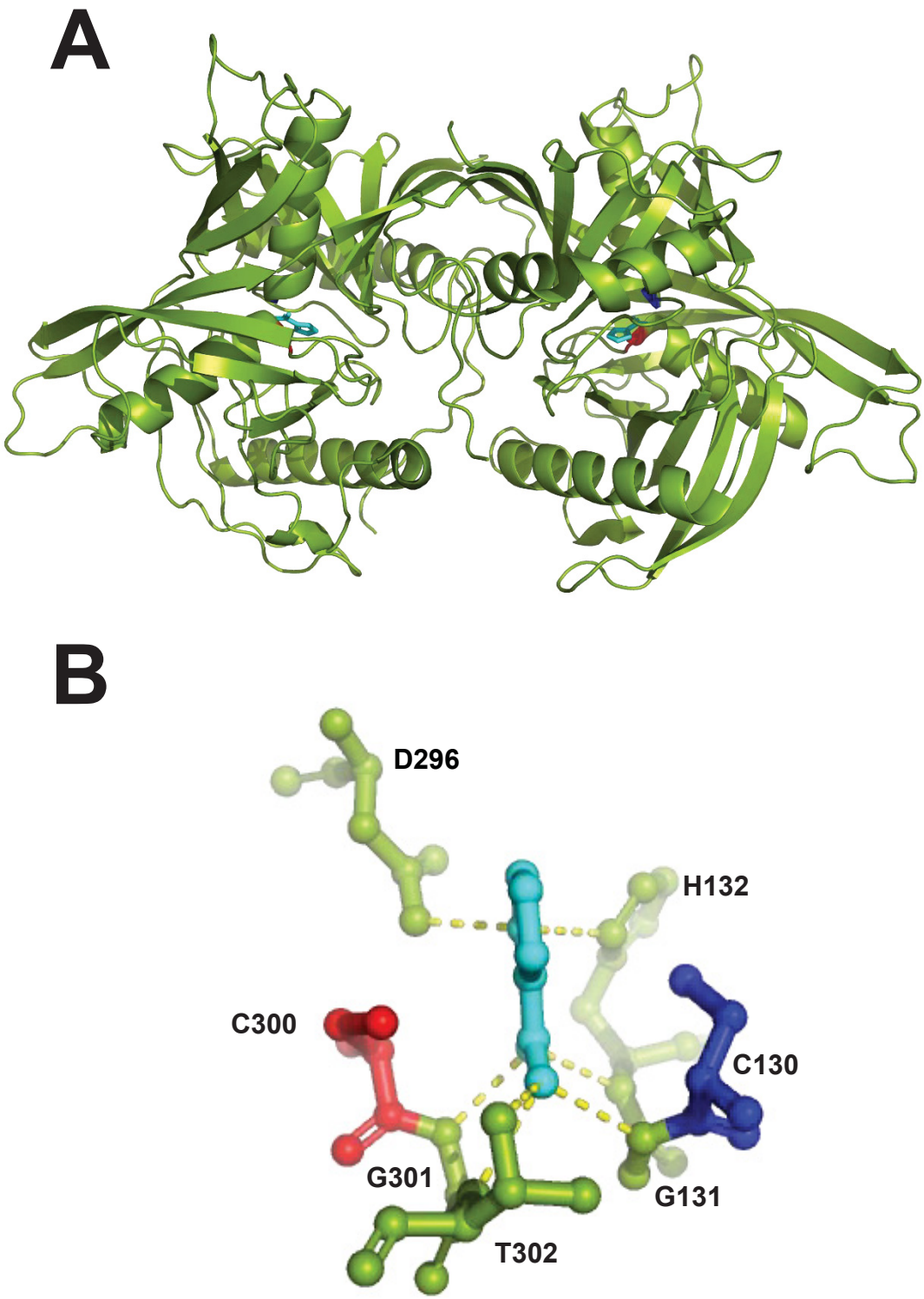

Figure 1.2 Active site of proline racemase from *T. cruzi* with pyrrole-2-carboxylic acid bound. (A) Dimeric PR with each protomer (green) bound to one molecule of pyrrole-2-carboxylic acid. (B) The bound *aci*-carboxylate analogue, pyrrole-2-carboxylic acid (cyan) is stabilised by various hydrogen bonding interactions from the active site residues: D296, H132, G131, G301 and T302, all shown in green. The catalytic residues, C130 and C300 are shown in blue and red, respectively [PDB entry 1W62 (Buschiazzo *et al*., 2006)].

The structure of the active site of the enzyme with PYC bound revealed that the surrounding amino acid residues, Gly-131, His-132, Asp-296, Gly-301 and Tyr-302, are oriented to participate in the stabilisation of the ligand through hydrogen bonding interactions (Buschiazzo *et al.*, 2006). The sulfhydryl groups of the catalytic residues, Cys-130 and Cys-300, are positioned at 3.4-3.5 Å from either side of the C_α of PYC (equivalent to the C_α of proline), thus favouring the protonation/deprotonation of the C_α. These two residues also play a critical role in stabilising the planar conformation of the intermediate formed during the racemisation reaction of proline (Buschiazzo *et al.*, 2006). The nitrogen of the pyrrole ring is at hydrogen bonding-distances from His-132 (3.1 Å) and Asp-296 (3.0 Å) and the pyrrole ring has hydrophobic contacts with Phe-102 and Phe-290 (Buschiazzo *et al.*, 2006). The carboxylate group of PYC is secured by five hydrogen bonds leading to a tetrahedral configuration which stabilises the negative charge of the deprotonated intermediate through resonance (Buschiazzo *et al.*, 2006). Currently, there is no crystal structure for PR bound to the substrate proline, but various studies have proposed models based on the existing crystal structure with PYC. The most widely accepted hypothesis states that both His-132 and Asp-296 play important roles in the catalytic function of the enzyme, though not directly involved in catalysis (Rubinstein & Major, 2009). Since the amine group ($pK_a \sim 9.6$) of the zwitterionic proline (at pH 8.0) can be susceptible to deprotonation, it is proposed to be stabilised by hydrogen bonding interactions with His-132 and Asp-296, thus preventing any changes in orientation of proline within the active site that would promote the deprotonation of the amine group (Rubinstein & Major, 2009). These tight interactions within the active site of the enzyme enable the deprotonation of the C_α centre of proline in the absence of a cofactor.

1.1.4 Mechanism of PR catalysis

Racemisation reactions involving a change in the stereochemistry at the C_α-centre can proceed by two possible mechanisms as proposed by Cardinale & Abeles: a one-base mechanism or a two-base mechanism (1968). The one-base mechanism involves the abstraction of the C_α-hydrogen by an enzymatic Brønsted base generating a carbanionic intermediate. The conjugate acid of the Brønsted base then donates a proton to the C_α-centre forming the product isomer. But in this mechanism, the Brønsted base is positioned such that protonation of the C_α may occur stereo-randomely. The two-base mechanism utilises two enzymatic Brønsted bases that are located such that one base removes the C_α-hydrogen of one specific substrate stereoisomer and the conjugate acid of the other Brønsted base protonates the C_α to yield only the corresponding enantiomer. The roles of the two enzymatic Brønsted bases are reversed when the other enantiomer is the substrate (Cardinale & Abeles, 1968).

Deuterium and tritium exchange experiments can be conducted to distinguish between these two types of mechanisms (Rose, 1966). In the case of the one-base mechanism, the rate of deuterium incorporation into the stereoisomers will be greater than that of their interconversion. Whereas, if the rate of deuterium incorporation is the same as the rate of the interconversion of the isomers, irrespective of which isomer is the substrate, it implies a two-base mechanism. Also, for reactions proceeding without the requirement of a coenzyme, the two-base mechanism offers a better explanation due to a more rigid arrangement of the substrate within the active site (Cardinale & Abeles, 1968).

Extensive deuterium exchange experiments suggested that PR follows a two-

base mechanism to catalyse the racemisation of L- and D-proline (**Scheme 1.4**) (Rudnick & Abeles, 1975). Two monoprotonated amino acid residues were predicted to be present in the active site to facilitate the interconversion of L- and D-proline (Rudnick & Abeles, 1975). These turned out to be the sulfhydryl groups of two cysteine residues, which acted as Brønsted acid-base catalysts. First, the deprotonated cysteine residue abstracts the C_α-proton of proline, forming an *aci*-carboxylate intermediate which is stabilised by hydrogen bonding interactions with amino acid residues within the active site. The conjugate acid of the second cysteine residue then donates a proton to the C_α-centre of proline from the opposite side, thus effecting the stereoinversion of the C_α-centre of proline (Rudnick & Abeles, 1975). Hence, the two cysteine residues present at the active site of PR, Cys-130 and Cys-300, are alternatively protonated through exchange of protons with the solvent, depending on the specific stereoisomer of proline that binds (Rudnick & Abeles, 1975). Mutagenesis studies showed that point mutations at positions 300 and 130 lead to negligible or total loss of activity, suggesting that Cys-130 and Cys-300 are critical for catalysis by PR. Thus, in solution, two populations of enzymes exist in equilibrium, one that binds L-proline and the other that binds D-proline (Fisher *et al.*, 1986). When Cys-300 is deprotonated and Cys-130 is protonated, D-proline binds at the active site; and when Cys-130 is deprotonated and Cys-300 is protonated, L-proline binds at the active site (Rubinstein & Major, 2009).

1.1.5 Substrates and inhibitors of PR

PR has high substrate specificity towards L- and D-proline (K_m = 2.9 mM and 2.5, respectively, Fisher *et al.,* 1986), which are the natural substrates (Cardinale & Abeles, 1968). PR showed very low levels of catalysis for the racemisation of hydroxy-L-proline (2%) and allohydroxy-D-proline (5%) relative to L-proline

Scheme 1.4 Two-base mechanism of proline racemase-catalysed reaction

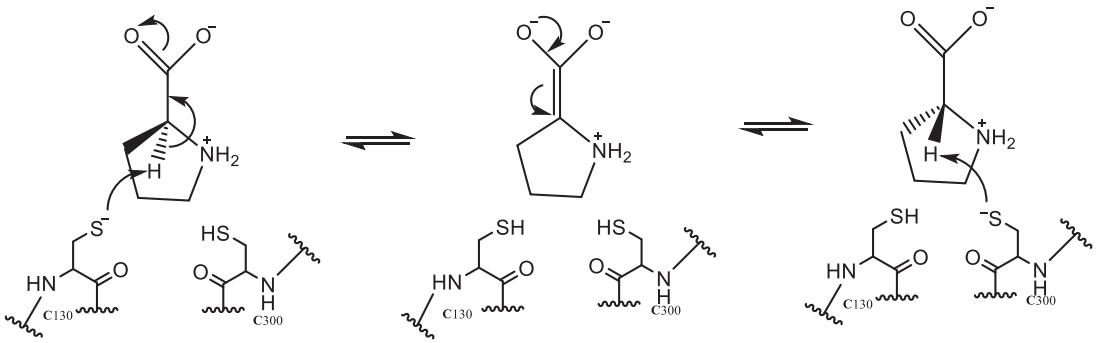

(Cardinale & Abeles, 1968). Early inhibition studies of PR catalysis by amino acids such as glycine, alanine and aspartic acid resulted in negligible to no inhibition (**Table 1.1**). Pipecolic acid, a six-membered ring analogue of proline, showed 18% inhibition consistent with weak binding (Cardinale & Abeles, 1968). The *aci*-carboxylate intermediate analogue, pyrrole-2-carboxylic acid showed maximum inhibition of 98% with a competitive binding constant (K_i) of 0.7 mM, by far the best inhibitor of PR catalysis reported (Cardinale & Abeles, 1968). Δ-1-pyrroline-2-carboxylate, another aci-carboxylate intermediate showed similar inhibition to pyrrole-2-carboxylic acid (Keenan & Alworth, 1974). 2-Thiophenecarboxylic acid, which has a sulphur in the position of the nitrogen of PYC, inhibited the activity of PR by 73%. Maleic acid (93% inhibition) and sarcosine (54% inhibition) also inhibited PR catalysis (Cardinale & Abeles, 1968). A four-membered ring analogue of proline, azetidine-2-carboxylic acid, was also reported to be a substrate of PR (Conti *et al.*, 2011). Iodoacetate inactivated PR catalysis, with a binding constant of 1.3 mM (Rudnick & Abeles, 1975), as would be expected since the Cys residues are critical for catalysis. To investigate the role of $-COO^-$ group in iodoacetate, inhibition by iodoacetamide (with $-CONH_2$) was examined and showed similar inactivation of PR with a binding constant of 1.6 mM. This observation suggested that the carboxyl group does not play a major role in inactivation (Rudnick & Abeles, 1975).

1.2 Temperature-dependence of enzyme catalysis

Enzymes are catalysts that are known to decrease the energy barrier of a reaction, thus enhancing the rate of the reaction. Organisms adapt to different temperatures, broadly classified into psychrophilic (−20 to +10 °C), mesophilic (20 to 45 °C) and thermophilic (50 to 122 °C). Thus, enzymes have evolved to function at studied. Changes in temperature can affect higher orders of protein

Table 1.1 List of inhibitors of proline racemase catalysis[a]

Inhibitor	% Inhibition
pyrrole-2-carboxylic acid 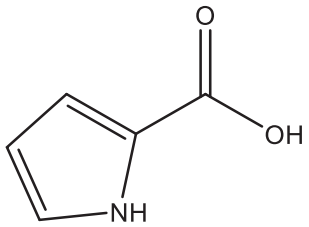 (K_i = 0.7 mM)	98
Δ-1-pyrroline-2-carboxylate 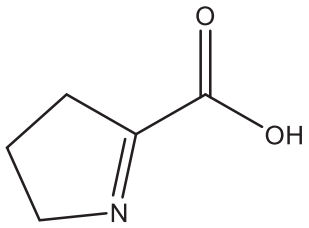	100
2-thiophenecarboxylic acid 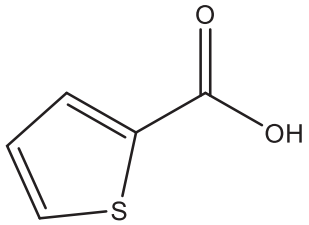	73
maleic acid 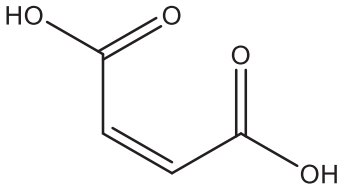	93
pipecolic acid 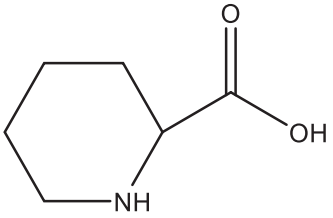	18
azetidine-2-carboxylic acid 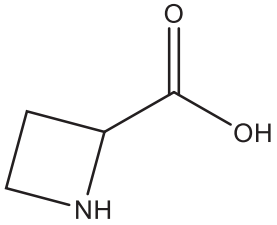	-
sarcosine 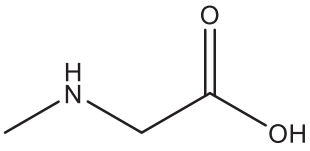	54

a from references Cardinale & Abeles, 1968, Keenan & Alworth, 1974 and Conti *et al.*, 2011

these temperatures and the effect of temperature on enzyme catalysis has been widely structure, in turn affecting enzyme-substrate complex formation (Low *et al*., 1973). The other major effect is on the formation of the activated enzyme-substrate complex or the transition state complex, which can be attributed to changes in the enthalpy ($\Delta H^{\ddagger}$) and entropy ($\Delta S^{\ddagger}$) of activation (Low *et al*., 1973). The activation free energies ($\Delta G^{\ddagger}$) of psychrophilic enzymes were found to be less than those of mesophilic enzymes (Low *et al*., 1973). This decrease in $\Delta G^{\ddagger}$ arises from the difference in $\Delta H^{\ddagger}$ (~3.4 kcal/mol) which can arise due to changes in internal structure of the protein, typically outside the conserved active site (Low *et al*., 1973).

On the other hand, thermophilic enzymes have decreased rates and, hence, increased $\Delta G^{\ddagger}$ compared to their mesophilic counterparts. For example, a thermophilic variant of glyceraldehyde-3-phosphate dehydrogenase (GAPDH) exhibited a 50% decrease in k_{cat} relative to a mesophilic variant (Thomas & Scopes, 1998). Exceptions to this have also been observed with 3-phosphoglycerate kinase (PGK), where an unusually high k_{cat} was reported for the thermophilic enzyme compared to the mesophilic enzyme (Thomas & Scopes, 1998).

Enzyme reactions tend to double in rate with every 10 °C increase in temperature (Wolfenden *et al.*, 1999). This value might be higher for single-substrate reactions and slow-hydrolytic reactions (Wolfenden *et al.*, 1999). The ratio of the rate constant of an enzyme-catalysed reaction (k_{cat}) to the rate constant of the corresponding uncatalyzed reaction (k_{non}) is defined as the rate enhancement (k_{cat}/k_{non}) brought about by an enzyme. A general observation with rate enhancements is that decreasing temperatures lead to increasing k_{cat}/k_{non} values (Snider *et al.*, 2000). But, the catalytic efficiency (k_{cat}/K_m) of the enzyme over different temperatures remains constant since the increase in the rate constant of the reaction (k_{cat}) with increasing

temperatures is compensated by the decreasing affinity of the substrate, i.e., increasing K_m (Wolfenden *et al.*, 1999). A study with cytidine deaminase showed such trends in the kinetic constants and a temperature-dependence study revealed that $\Delta G^{\ddagger}$ is mostly enthalpic in origin with a $\Delta H^{\ddagger}$ value of −20.1 kcal/mol and a $T\Delta S^{\ddagger}$ value of only 1.6 kcal/mol at 25 °C (Snider *et al.*, 2000). This is in accord with another study on α-glucosidase (Wolfenden *et al.*, 1999). An increase in affinity for the transition state (or decrease in K_{tx} - see below) with decreasing temperature is observed due to loss of enthalpy that can further be due to electrostatic and hydrogen-bonding interactions formed in the transition state complex (Bearne & Wolfenden, 1997; Kati & Wolfenden, 1989).

1.3 Thermodynamics of enzyme catalysis

1.3.1 Transition state stabilisation

The rate enhancements afforded by enzymes is said to be due to greater binding affinity for the altered substrate in the transition state (TS) (Pauling, 1948). Various studies unravelling enzyme catalysis and mechanisms are in accord with this proposal (Wolfenden 1969; Wolfenden, 1976; Lienhard, 1973; Schramm, 1998; Amyes & Richard, 2013). To quantify this transition state affinity for an enzyme, Wolfenden proposed that a thermodynamic cycle can be designed for a one-substrate reaction and that TS theory could be applied (Wolfenden, 1972; Wolfenden, 1969). The thermodynamic cycle comprises an equilibrium that exists between the dissociation of enzyme-substrate complex (ES, K_s) and the activated enzyme-substrate complex ($ES^{\ddagger}$, $K_{cat}^{\ddagger}$), the non-enzymatic formation of TS ($S^{\ddagger}$, $K_{non}^{\ddagger}$) and finally, the hypothetical equilibrium constant for binding of the TS to free enzyme (K_{tx}) (**Scheme 1.5**). These equilibrium constants are related by **equation 1.1**.

Scheme 1.5 Thermodynamic cycle representing the equilibria between the enzymatic and non-enzymatic reactions

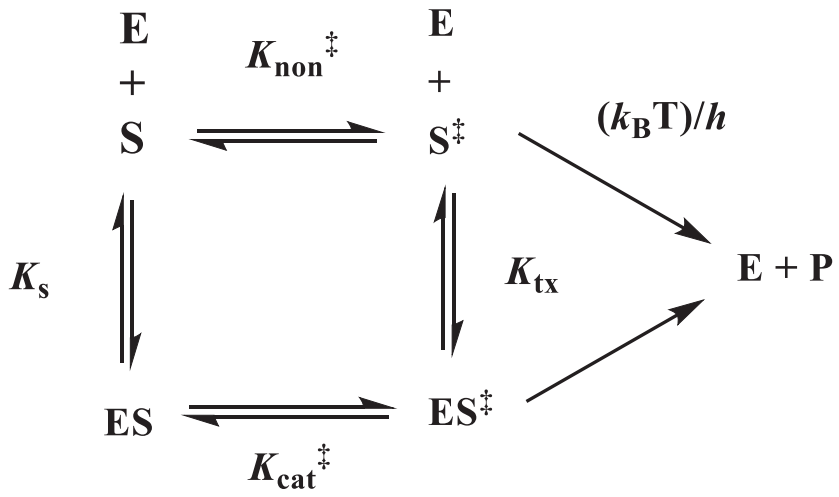

$$\frac{K_{tx}}{K_s} = \frac{k^{\ddagger}_{non}}{k^{\ddagger}_{cat}} \quad (1.1)$$

According to the TS theory, the equilibrium constant between the reactant and the transition state ($K^{\ddagger}$) can be determined from **equation 1.2**, where k is the first order rate constant, $k_B T/h$ is the universal frequency factor (k_B = Boltzmann constant, h = Planck's constant, T = absolute temperature) (Wolfenden, 1972). Substituting $\Delta G^{\ddagger} = -RT\ln K^{\ddagger}$, since $K^{\ddagger}$ is an association constant, the first order rate can be expressed in terms of free energy of activation ($\Delta G^{\ddagger}$) as represented in **equation 1.3**.

$$k = \left(\frac{k_B T}{h}\right) K^{\ddagger} \quad (1.2)$$

$$k = \left(\frac{k_B T}{h}\right) e^{\left(\frac{-\Delta G^{\ddagger}}{RT}\right)} \quad (1.3)$$

The virtual dissociation constant, K_{tx}, can then be determined by expressing $K_{cat}^{\ddagger}$ and $K_{non}^{\ddagger}$ in terms of k_{cat} and k_{non}, respectively, as shown in **equation 1.4**, where k_{non} is the first order rate constant for the non-enzymatic reaction and (k_{cat}/K_s) is the apparent second order rate constant for the corresponding enzymatic reaction.

$$K_{tx} = \frac{k_{non}}{(k_{cat}/K_s)} \quad (1.4)$$

From **equation 1.4**, the proficiency of the enzyme ($1/K_{tx}$) can be calculated which is the degree to which an enzyme stabilises the altered substrate in the TS compared to the substrate in the ground state (Radzicka & Wolfenden, 1995a). This approach is based on two main assumptions: one is that both the enzymatic and the non-enzymatic reactions proceed through the same transition state structures, and the other is that the rate-limiting step is the chemical step for the enzymatic reaction. There can be exceptions to these assumptions, where enzymatic reactions can be

limited by various other processes, such as product release or conformational changes. Thus, TS theory provides only a minimum estimate of the transition state stabilisation afforded by an enzyme (Wolfenden, 1972; Lienhard, 1973). Keeping these assumptions in mind, a free energy profile representing the energy path of both enzymatic and non-enzymatic reactions can be traced (**Figure 1.3**).

Kinetic studies with a variety of enzymes have revealed enzyme proficiencies ranging from 10^9 M^{-1} (carbonic anhydrase) to 10^{29} M^{-1} (alkylsulfatase) that correspond to −10 to −39.5 kcal/mol of ΔG_{tx}. In the case of PR, the rate enhancement of 10^{14} M^{-1} was reported by Williams *et. al.*, 2003.

1.3.2 **The role of entropy in enzyme catalysis**

$\Delta G^{\ddagger}$ is the sum of the contributions from the change in enthalpy ($\Delta H^{\ddagger}$) and the change in entropy of activation ($T\Delta S^{\ddagger}$) (**equation 1.5**).

$$\Delta G^{\ddagger} = \Delta H^{\ddagger} + T\Delta S^{\ddagger} \quad (1.5)$$

The contribution of entropy to the free energy of activation is often less than enthalpic contributions (Wolfenden *et al.*, 1999). Specific binding of the enzyme to the substrate in solution decreases the free energy of activation ($\Delta G^{\ddagger}$) (Page & Jencks, 1971). In solution, substrate molecules are expected to possess high entropy due to contributions from the translational, rotational and vibrational degrees of freedom. The rate enhancement of reactions of small molecule substrates by Bronsted acid-base catalysts in solution depends on the effective molarity of the catalyst(s) in solution. This effective molarity can range from 1 to 55 M, corresponding to 8 entropy units.

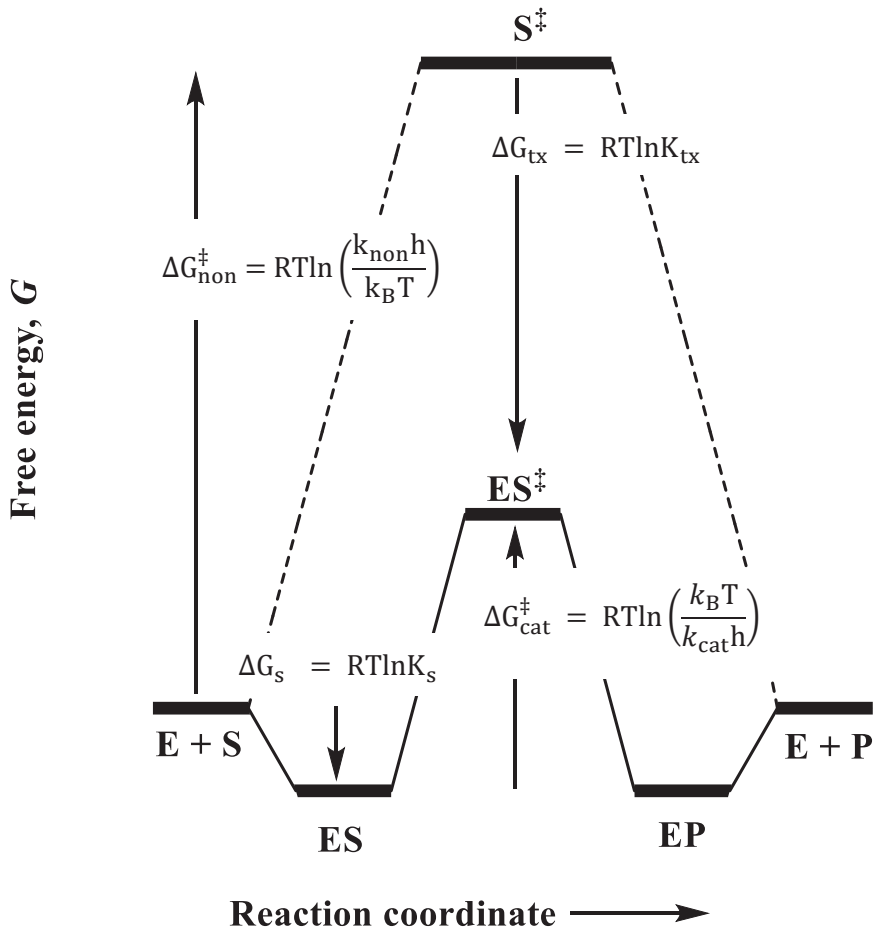

Figure 1.3 Free energy profile for enzymatic and non-enzymatic conversion of substrate to product. ΔG_{tx} is the free energy of transition state stabilisation provided by the enzyme.

There are two possible factors that contribute to the effective molarity: first, the rate of diffusion of the molecules in solution and second, the orientation of the molecules (Koshland, 1962; Bender, 1964; Jencks, 1969).

The entropy of substrate molecules in solution is reduced upon binding to an enzyme (Villa *et al.*, 2000). Binding reduces the amount of spatial freedom the substrate has and fixes the substrate in a favourable conformation for reaction (Villa *et al.*, 2000). Since this loss in entropy is highly unfavourable, it is referred to as an "entropic cost" that the enzymatic system pays to enhance the rate of the reaction. Jencks proposed a phenomenon called the Circe effect, where the substrate is destabilised by the enzyme from its ground state such that the entropy of the substrate is largely decreased by restricting the motion of the substrate while increasing the proximity of the reactive groups (Page and Jencks, 1971). Evidence for this effect was observed with orotidine-5-phosphate decarboxylase; however, Kazemi *et al*., 2016 conducted a study on cytidine deaminase that did not support this hypothesis of Jencks's, where a preorganised active site was responsible for stabilising the reaction path rather than utilising the change in free energy to pay "entropic costs", as suggested by the Circe effect. Though most of the entropic contributions to enzyme-substrate complex formation are external (result from the loss of three translational and three rotational degrees of freedom, Page & Jencks, 1971), internal bond rotations and vibrations also contribute to such large rate enhancements (O'Neal & Benson, 1970).

1.4 Thesis overview

PR is a very proficient enzyme with high affinity for the altered substrate in the transition state as suggested by the affinity of the transition state analogue inhibitor pyrrole-2-carboxylic acid (0.7 mM) for *Cs*PR (Cardinale & Abeles, 1968; Keenan &

Alworth, 1974). This early study led to using PR as a model enzyme to gain insight into transition state stabilisation by enzymes. Extensive research on PR was conducted by Knowles (1986) to investigate the energetic contributions involved in PR-catalysed racemisation of proline. However, these studies did not specifically examine entropic effects in PR catalysis.

Cardinale & Abeles identified other inhibitors of *Cs*PR catalysis such as pipecolic acid, 2-thiophene carboxylic acid, maleic acid and sarcosine (Cardinale & Abeles, 1968). That most of these inhibitors contain an intact-ring structure led me to the question: How important is this ring structure of the substrate for *Cs*PR catalysis? To address this question, we designed a substrate analogue, *N*-ethyl-L-alanine (NEA), which was a "broken" ring relative to the structure of proline and explored its interaction with *Cs*PR.

To understand the temperature-dependence of PR catalysed reactions, I conducted kinetic studies with two variants of PR: *Cs*PR (mesophilic) and *Tl*PR (hyperthermophilic) (**Chapter 2**). Further, kinetic studies with the substrate analogue NEA were conducted to understand the effect of entropy on *Cs*PR catalysis (**Chapter 3**). A remarkable decrease in the efficiency of *Cs*PR-catalysed racemisation of NEA relative to that of proline led me to investigate steric effects on *Cs*PR catalysis using a spectrum of substrate analogues – pipecolic acid (a six-membered ring analogue of proline), *N*-methylalanine (NMA) and L-azetidine-2-carboxylic acid (ACA) (a four-membered ring analogue of proline) (**Chapter 4**). Surprising results from preliminary studies with NMA then finally led me to investigate the inhibition kinetics with NMA as an inhibitor of *Cs*PR catalysis (**Chapter 4**).

CHAPTER 2

KINETICS AND ENERGETICS OF THERMOPHILIC AND MESOPHILIC VARIANTS OF PROLINE RACEMASE: A COMPARATIVE STUDY

2.1 INTRODUCTION

Enzymes catalysing the same reaction have evolved over time to function at different temperatures. In general, thermophilic and mesophilic enzymes differ largely in terms of their thermodynamic contributions to reaction catalysis. Though thermophilic enzymes may be expressed in mesophilic organisms, as in this study where *Tl*PR is overproduced in *E. coli*., the thermophilic properties are retained showing that the protein sequence is responsible for the thermostability (Vieille & Zeikus, 2001). Though thermophilic enzymes have high sequence homologies with mesophilic enzymes, higher orders of enzyme structures vary resulting in higher thermostability of thermozymes (Low *et al.*, 1973). Some structural variations may include a tendency to form more disulphide bonds, to have more hydrogen bonds, and to have an increased number of proline residues, as well as more rigid packing of the secondary structures of the enzyme in thermophilic enzymes relative to their mesophilic counterparts (Santos *et al.*, 2011; D'Amico *et al.*, 2003). Apart from structural distinctions, these classes of enzymes also vary in terms of thermodynamic contributions to the reactions that they catalyse. Thermophilic enzymes show decreased free energies of activation relative to mesophilic enzymes, as seen with glyceraldehyde-3-phosphate dehydrogenase (Thomas & Scopes, 1998).

In this work, PR variants from two temperature adaptations were chosen for study: *Cs*PR from *Clostridium sticklandii*, a mesophile, and *Tl*PR from *Thermococcus litoralis*, a hyperthermophile. The optimal temperature for *Tl*PR function is 50 °C, whereas that of *Cs*PR is 37 °C (Watanabe *et al.*, 2015; Cardinale & Abeles, 1968). A

temperature-dependent study on *Tl*PR and *Cs*PR catalysis was conducted to unravel the thermodynamic differences between these two enzymes.

The Eyring-Polanyi equation (see **equation 2.2**) relates the rate constant (k_{cat}) of the enzyme-catalysed reaction to the free energy of activation ($\Delta G^{\ddagger}$) under the assumption that the change in enthalpy of activation ($\Delta H^{\ddagger}$) and the change in entropy of activation ($\Delta S^{\ddagger}$) are insensitive to temperature (Eyring, 1935). Determining these thermodynamic parameters would afford a better understanding of the kinetics and thermodynamics of thermophilic and mesophilic PR. The rationale for studying *Tl*PR was that, among all the PRs reported in the literature, *Tl*PR was shown to bind L-proline with the highest affinity of all PRs studied to date, i.e., with the lowest Michaelis constant (K_m) of 1.2 ± 0.1 mM (Watanabe *et al.*, 2015). Thus, it would be interesting to know if *Tl*PR provides a better model for studies with substrate analogues, since it apparently binds the substrate proline with higher affinity than *Cs*PR.

2.2 MATERIALS AND METHODS

2.2.1 General

L-Proline, D-proline, and all other reagents, unless mentioned otherwise, were purchased from Sigma-Aldrich Canada Ltd. (Oakville, ON, Canada). Circular dichroism (CD) experiments were conducted using a JASCO J-810 spectropolarimeter (Jasco Inc., Easton, MD), with a temperature-controlled jacketed cell holder.

2.2.2 Production and purification of *Cs*PR

Proline racemase from *Clostridium sticklandii* (*Cs*PR) was overproduced in and purified from *Escherichia coli* BL21(DE3) cells transformed with the pET-15b

plasmid containing the open reading frame (ORF) encoding *Cs*PR as a fusion protein with an *N*-terminal His_6-tag to facilitate protein purification (Harty *et al.*, 2014). To overproduce *Cs*PR, lysogeny broth media (LB, 2 × 5 mL) with ampicillin (100 µg/mL) was inoculated with single colonies of *E. coli* followed by overnight incubation at 37 °C with constant shaking at 220 rpm. This pre-inoculum was used to inoculate 1 L of LB media containing ampicillin (100 µg/mL), which was further incubated at 37 °C until the exponential growth phase was attained (OD_{600} ≈ 0.6). Gene expression was induced with isopropyl β-D-1-thiogalactopyranoside (IPTG, 1 mM) and the culture incubated at 37 °C for 6 h with continuous shaking at 220 rpm. The cells were collected by centrifugation (1,541 × *g*, 10 min, 4 °C) and stored at −20 °C. To lyse the cells, the cell pellet was resuspended in 20-25 mL of lysis buffer [Tris-HCl buffer (20 mM, pH 7.9) containing NaCl (0.5 M) and imidazole (5 mM)] and was sonicated (5 × 30 s bursts with ~ 1 min cooling intervals) using a Branson Sonifier 250 (power setting of 5.5). The lysed cells were then centrifuged (40,000 × *g*, 30 min, 4 °C) and the clarified cell lysate (supernatant) was collected for further purification. The His_6-*Cs*PR fusion protein was purified by Ni^{2+}-affinity chromatography using Novagen protocols (Novagen, 2003). The supernatant (~10 mL) was added to 2.5 mL of resin (Novagen His-Bind Resin, EMD Chemicals Inc., San Deigo, CA, USA) in a plastic column, followed by 25 mL of binding buffer [Tris-HCl (20 mM, pH 7.9) containing NaCl (0.5 M) and imidazole (5 mM)] and then by 10 mL of wash buffer [Tris-HCl (20 mM, pH 7.9) containing NaCl (0.5 M) and imidazole (60 mM)]. The protein was eluted with 7.5 mL of strip buffer [Tris-HCl (20 mM, pH 7.9) containing NaCl (0.5 M) and EDTA (100 mM)]. The eluted protein was dialysed against Tris-HCl buffer (100 mM, pH 8.0) containing EDTA (8 mM) and stored at −20 °C.

2.2.3 Cloning of the *Tl*PR gene

The ORF of the gene encoding the proline racemase-like enzyme from *Thermococcus litoralis* (*Tl*PR, accession number: CP006670), inserted into the pET-15b plasmid, was commercially synthesised (Bio Basic Inc., Markham ON, Canada). This construct encodes *Tl*PR as a fusion protein with an *N*-terminal His_6-tag. The synthesised *Tl*PR gene contained rare codons (CGG, AGG, AGA, GGA, GGG, AUA, CUA, CCC and, ACG) in the context of the translation machinery of *E. coli*. To overcome this codon bias, an additional plasmid, pLysRARE, with genes encoding the less abundant tRNAs, was used to aid overproduction of the desired protein. Competent *E. coli* DH5α cells were transformed with the pET-15b-*Tl*PR plasmid for DNA propagation followed by transformation of *E. coli* BL21(DE3) cells with both the pET-15b-*Tl*PR and pLysRARE plasmids for protein production. The transformed cells were stored as glycerol stocks (7.5% glycerol) at −80 °C.

2.2.4 Production and purification of *Tl*PR

*Tl*PR was overproduced in and purified from *E. coli* BL21(DE3) cells transformed with the pET-15b-*Tl*PR and pLysRARE plasmids. Cells were grown in LB media (1 L) with ampicillin (100 μg/mL) and chloramphenicol (34 μg/mL), similar to the protocol described for the purification of *Cs*PR. After 7-8 h of growth, the cells were collected by centrifugation (1,541 × *g*, 10 min, 4 °C) and stored at −20 °C. The frozen cell pellet was then thawed and resuspended in lysis buffer [Tris-HCl (20 mM, pH 7.9) containing NaCl (0.5 M) and imidazole (5 mM)] followed by sonication (5 × 30 s bursts with ~ 1 min cooling intervals) using a Branson Sonifier 250 (power setting of 5.5). The sonicated mixture was centrifuged (40,000 × *g*, 30

min, 4 °C) to separate cell debris from the soluble fraction. The clear supernatant containing soluble His_6-*Tl*PR protein was subjected to heat purification by heating at 70 °C for 20 min followed by cooling on ice for 20 min. The denatured proteins were then separated using centrifugation (40,000 × *g*, 30 min, 4 °C). The soluble fraction (supernatant) was then subjected to Ni^{2+}-affinity chromatography as described for *Cs*PR. *Tl*PR was eluted by gradient elution using elution buffers [Tris-HCl (20 mM, pH 7.9) containing NaCl (0.5 M)] with increasing concentrations of imidazole (90 mM, 250 mM and 500 mM). The pure protein eluted 250 mM imidazole concentration was then dialysed against Tris-HCl (50 mM, pH 8.0) containing glycerol (10%), and stored at −80 °C.

2.2.5 Circular dichroism spectroscopy-based PR assays for temperature-dependence studies

The temperature-dependence of the reactions catalysed by *Cs*PR and *Tl*PR was followed using circular dichroism (CD)-based assays. Assays were conducted at a range of temperatures for both *Cs*PR (288-320 K) and *Tl*PR (293-343 K). For *Cs*PR assays, the reaction mixture including assay buffer [Tris-HCl, (100 mM, pH 8.0) containing EDTA (8 mM)] with L- or D-proline as the substrate (0.5 mM – 120 mM final concentration) was pre-incubated at the corresponding temperatures for 5 min followed by initiation of the reaction by addition of *Cs*PR (150 nM, final concentration) such that the final volume of the reaction mixture was 500 µL. An aliquot of the reaction mixture (300 µL) was then transferred to a quartz cuvette with a 0.1-cm light path to measure the change in ellipticity at 220 nm with time (over 5 min). These changes in ellipticity were used to calculate velocities using the molar ellipticity values ($[\theta]_{220}$) of 6800 (± 54) and −6800 (± 54) for L- and D-proline,

respectively (Harty *et al.*, 2014). *Tl*PR assays were conducted as described for *Cs*PR, except that the assay buffer was Tris-HCl buffer (50 mM, pH 8.0).

2.2.6 Data analysis

The purity of the proteins was analysed using SDS-PAGE (10% acrylamide gel) with Coomassie brilliant blue R-250 staining (**Figure 2.1**). The concentration of *Cs*PR was determined by the Bradford method (Bradford, 1976) using the Bio-Rad Protein Assay dye reagent (Bio-Rad Laboratories, Missisauga, ON, Canada) with bovine serum albumin standards (0.5-5 mg/mL) or using the Beer-Lambert law by measuring absorbance at 280 nm and using the molar extinction coefficient of 14,900 $M^{-1}cm^{-1}$, calculated using the ProtPram tool (Gasteiger *et al.*, 2005, https://web.expasy.org/protparam/). The concentration of *Tl*PR was determined by the Bradford method, as mentioned for *Cs*PR. The V_{max} and K_m values for *Cs*PR and *Tl*PR assays were determined by fitting **equation. 2.1** (Michaelis and Menten, 1913) to the initial velocities (v_i) using non-linear regression analysis and KaleidaGraph v. 4.03 from Synergy software (Reading, PA). k_{cat} values were then determined by dividing V_{max} values by the concentration of the enzyme. All kinetic parameters were determined in triplicate and the averages with standard deviations from the mean are reported. Eyring-Polanyi and van't Hoff plots were analysed by fitting **equations. 2.2** and **2.3** to the temperature dependence of the rate constants and equilibrium constants, respectively.

$$v_i = \frac{V_{max}[S]}{K_m + [S]} \tag{2.1}$$

$$ln\frac{k}{T} = \frac{-\Delta H^{\ddagger}}{R}.\frac{1}{T} + ln\frac{k_B}{h} + \frac{\Delta S^{\ddagger}}{R} \tag{2.2}$$

$$ln\, K_m = \frac{\Delta H}{RT} - \frac{\Delta S}{R} \tag{2.3}$$

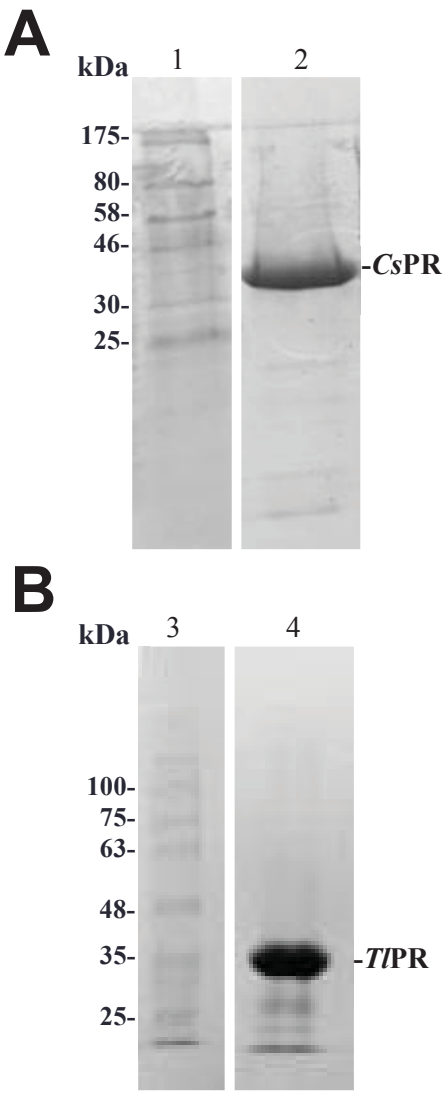

Figure 2.1 Images of SDS-PAGE gels (12%). Lane 1 shows molecular weight marker and lane 2 shows purified recombinant His_6-*Cs*PR (**A**). Lane 3 shows molecular marker and lane 4 shows the purified recombinant His_6-*Tl*PR (**B**).

2.3 RESULTS

2.3.1 Eyring-Polanyi and van't Hoff plots for *Cs*PR catalysis

The enzyme efficiencies (k_{cat}/K_m) of the reactions catalysed by *Cs*PR with L- and D-proline as the substrates were independent of temperature (**Table 2.1**), in accordance with Wolfenden *et al.*, 1999. The affinity of *Cs*PR for substrate was found to decrease with increased temperature, as evidenced by the observed increase in K_m values at higher temperatures. This effect was compensated by an increase in k_{cat} values, such that the efficiency of the reaction remained invariant with temperature. Eyring-Polanyi and van't Hoff equations describe the temperature dependence of rate constants and equilibrium constants, respectively. The kinetic parameters, k_{cat} and K_m, determined for *Cs*PR-catalysed reactions at temperatures from 288 to 320 K showed a linear dependence on temperature (**Figures 2.2** and **2.3**). Assuming that the thermodynamic parameters remain constant within this temperature range (Eyring, 1935) (which appears to be a valid assumption based on the linearity of the plots), the enthalpies of activation ($\Delta H^{\ddagger}$) of *Cs*PR-catalysed racemisation of L-proline (−14.7 kcal/mol) and D-proline (−12.8 kcal/mol) differed by only ~2 kcal/mol and their corresponding entropies of activation ($\Delta S^{\ddagger}$) were −0.003 kcal/mol·K and −0.010 kcal/mol·K, respectively.

2.3.2 Eyring-Polanyi and van't Hoff plots for *Tl*PR catalysis

To study the dependence of *Tl*PR catalysis on temperature, the kinetic parameters, k_{cat} and K_m, were plotted as a function of the reciprocal of temperature,

Table 2.1 Kinetic parameters for the *Cs*PR-catalysed racemisation of L-proline and D-proline by *Cs*PR at different temperatures.

L-proline			
T (K)	**k_{cat} (s^{-1})**	**K_m (mM)**	**k_{cat}/K_m (s^{-1} mM^{-1})**
288	12.4 ± 0.1	1.5 ± 0.2	8.2 ± 0.1
295	14.5 ± 1.6	1.7 ± 0.5	8.5 ± 0.3
300	33.6 ± 5.7	3.2 ± 0.9	10.50 ± 0.3
305	43.40 ± 0.01	6.0 ± 0.2	7.23 ± 0.03
310	82.8 ± 0.5	9.5 ± 0.5	8.71 ± 0.05
315	111.4 ± 1.6	11.9 ± 0.8	9.36 ± 0.07
320	138.2 ± 7.5	19.1 ± 1.3	7.23 ± 0.09
D-proline			
T (K)	**k_{cat} (s^{-1})**	**K_m (mM)**	**k_{cat}/K_m (s^{-1} mM^{-1})**
288	7.2 ± 0.5	0.51 ± 0.03	14.4 ± 0.1
295	12.3 ± 1.9	0.88 ± 0.05	13.4 ± 0.2
300	14.6 ± 1.4	1.26 ± 0.05	9.1 ± 0.1
305	19.6 ± 1.8	1.8 ± 0.3	10.8 ± 0.1
310	45.6 ± 0.6	4.1 ± 0.6	11.2 ± 0.1
315	46.40 ± 5.07	4.4 ± 0.3	10.6 ± 0.1
320	72.6 ± 1.9	8.9 ± 0.2	8.15 ± 0.04

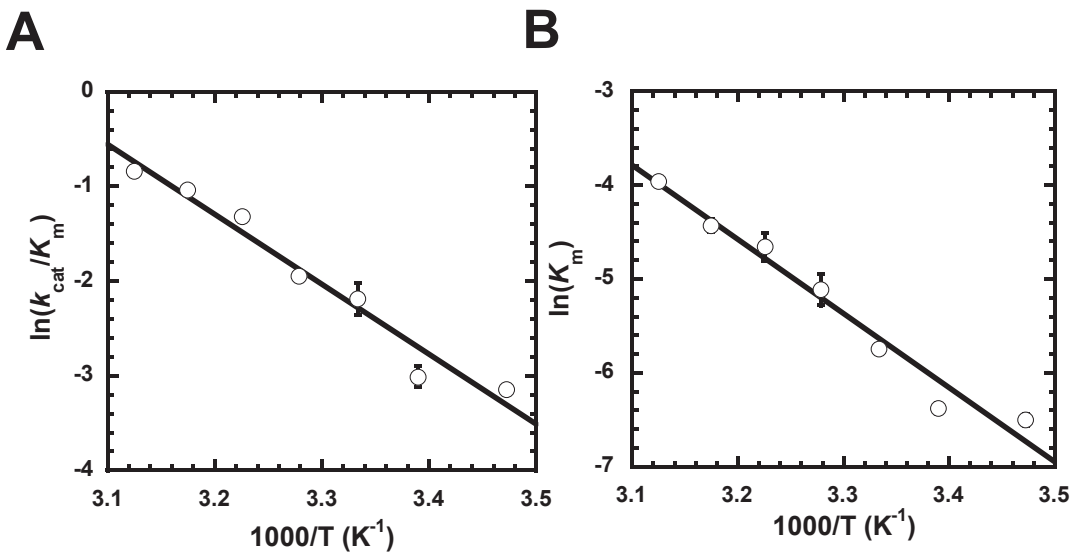

Figure 2.2 Temperature dependence of the kinetic parameters for the *Cs*PR-catalysed racemisation of L-proline. For the Eyring-Polanyi plot (**A**), the equation of the regression line is $ln\frac{k_{cat}}{T} = -7383.3\ (\pm 36.9)(1/T) + 22.3\ (\pm 1.8)$. For the van't Hoff plot (**B**), the equation of the regression line is $lnK_m = -7907.5\ (\pm 23.5)(1/T) + 20.7\ (\pm 2.1)$.

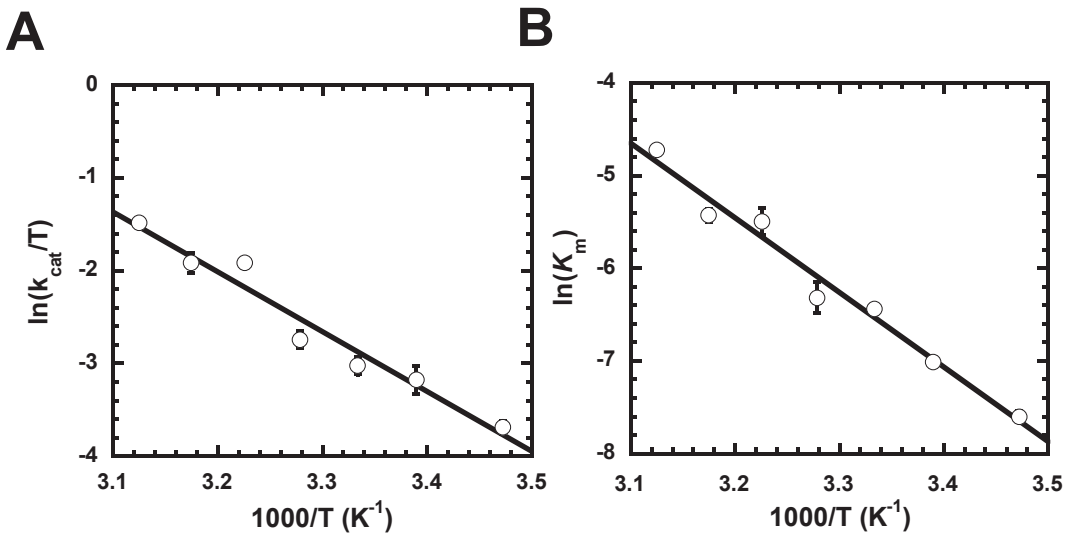

Figure 2.3 Temperature dependence of the kinetic parameters for the *Cs*PR-catalysed racemisation of D-proline. For the Eyring-Polanyi plot (**A**), the equation of the regression line is $ln\frac{k_{cat}}{T} = -6451.9\ (\pm 33.2)(1/T) + 18.6\ (\pm 3.2)$. For the van't Hoff plot (**B**), the equation of the regression line is $lnK_m = -8049.4\ (\pm 32.5)(1/T) + 20.3\ (\pm 2.6)$.

and linear relationships were observed, in accordance with the Eyring-Polanyi and van't Hoff equations (**Figures 2.4** and **2.5**). Again, the enzyme efficiencies for the *Tl*PR-catalysed reactions with L- and D-proline were constant over the temperature range studied (293-343 K) (**Table 2.2**). $\Delta H^{\ddagger}$ values for the racemisation both L-proline (14.05 kcal/mol) and D-proline (13.5 kcal/mol) were similar with only a slight difference of ~ 0.5 kcal/mol. The $\Delta S^{\ddagger}$ value for the racemisation of L-proline was −0.004 kcal/mol·K and that of D-proline was −0.007 kcal/mol·K.

2.3.3 Free energy profiles for *Cs*PR and *Tl*PR catalysed racemisation of L- and D-proline

When the free energy of activation and binding free energies calculated from change in enthalpy and entropy at 25 °C (**equations 2.2** and **2.3**) were plotted on a reaction coordinate diagram (**Figure 2.6**), the resulting free energy diagrams were remarkably similar for *Cs*PR and *Tl*PR. No significant difference was observed in $\Delta G^{\ddagger}$ for *Cs*PR and *Tl*PR, (calculated from change in enthalpy and entropy at 25 °C) (**Table 2.3** and **Figure 2.6**). The binding energy (calculated from the Michaelis constant, K_m) of *Cs*PR with L-proline is lower than that of *Tl*PR, by ~2.2 kcal/mol, implying that the mesophilic variant of PR (*Cs*PR) binds proline better than the thermophilic enzyme (*Tl*PR).

2.4 DISCUSSION

Differences in catalytic efficiencies of thermophilic enzymes and mesophilic enzymes have been studied extensively in the past (Beadle *et al.*, 1999; Wolf-Watz *et al*, 2004; Sundaram *et al.,*1980). In the present study, the hyperthermophilic *Tl*PR showed greater turnover of proline (in both reaction directions) than the mesophillic

Table 2.2 Kinetic parameters for the *Tl*PR-catalysed racemisation of L-proline and D-proline by *Tl*PR at different temperatures.

L-proline			
T (K)	**k_{cat} (s^{-1})**	**K_m (mM)**	**k_{cat}/K_m ($mM^{-1}s^{-1}$)**
293	21.2 ± 2.8	2.1 ± 0.9	9.9 ± 0.4
303	62.96 ± 1.20	6.8 ± 0.8	8.2 ± 0.1
313	139.9 ± 8.7	18.2 ± 2.5	7.7 ± 0.2
323	265.6 ± 15.0	31.2 ± 2.2	7.9 ± 0.1
333	500.0 ± 24.3	61.4 ± 2.7	8.14 ± 0.07
343	903.0 ± 16.1	109.2 ± 0.7	8.27 ± 0.02
D-proline			
T (K)	**k_{cat} (s^{-1})**	**K_m (mM)**	**k_{cat}/K_m ($mM^{-1}s^{-1}$)**
293	11.4 ± 0.6	1.4 ± 0.7	8.2 ± 0.5
303	32.3 ± 2.2	3.3 ± 0.4	9.8 ± 0.1
313	68.9 ± 1.5	7.1 ± 0.2	9.70 ± 0.07
323	126.8 ± 2.1	14.4 ± 1.0	8.81 ± 0.03
333	265.6 ± 3.4	30.8 ± 2.2	8.62 ± 0.07
343	392.5 ± 26.5	35.7 ± 1.5	10.99 ± 0.08

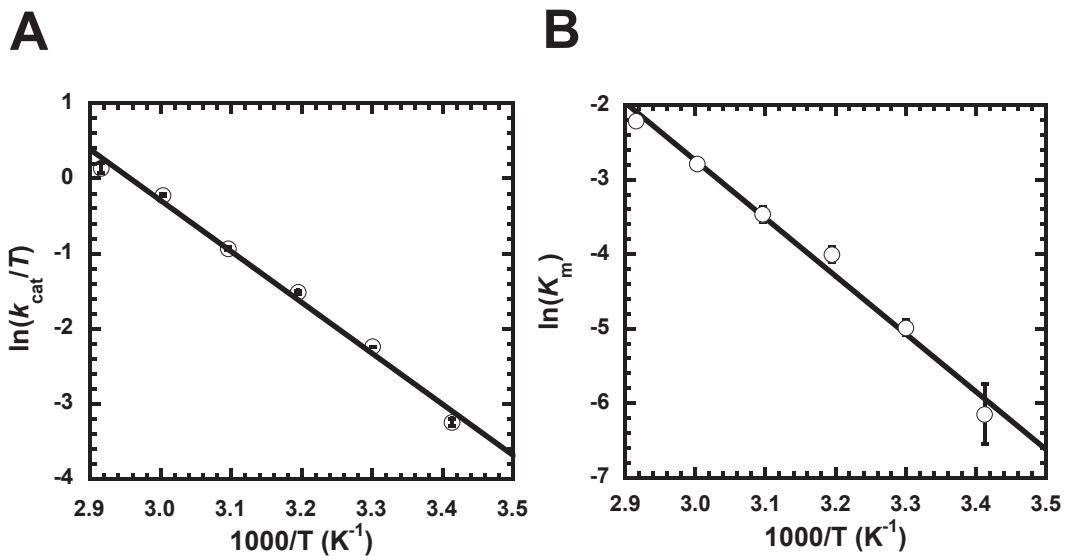

Figure 2.4 Temperature dependence of the kinetic parameters for the *Tl*PR-catalysed racemisation of L-proline. For the Eyring-Polanyi plot (**A**), the equation of the regression line is $ln\frac{k_{cat}}{T} = -7074.1\ (\pm 18.9)(1/T) + 21.7\ (\pm 3.2)$. For the van't Hoff plot (**B**), the equation of the regression line is $lnK_m = -7746.4\ (\pm 21.5)(1/T) + 20.7\ (\pm 2.1)$.

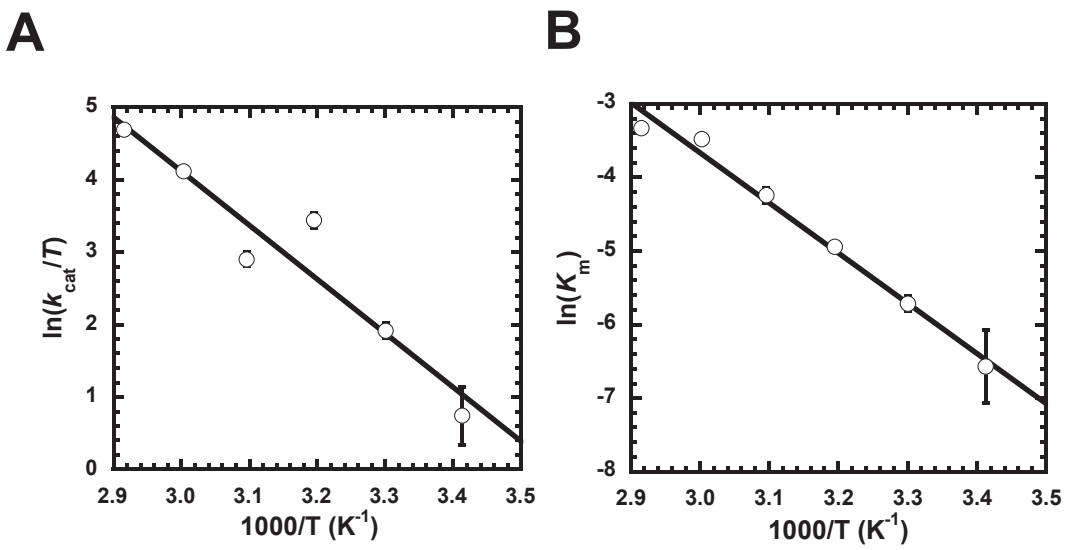

Figure 2.5 Temperature dependence of the kinetic parameters for the *Tl*PR-catalysed racemisation of D-proline. For the Eyring-Polanyi plot (**A**), the equation of the regression line is $ln\frac{k_{cat}}{T} = -6784.3\ (\pm 22.4)(1/T) + 20.1\ (\pm 2.2)$. For the van't Hoff plot (**B**), the equation of the regression line is $lnK_m = -6810.5\ (\pm 20.7)(1/T) + 16.8\ (\pm 3.2)$.

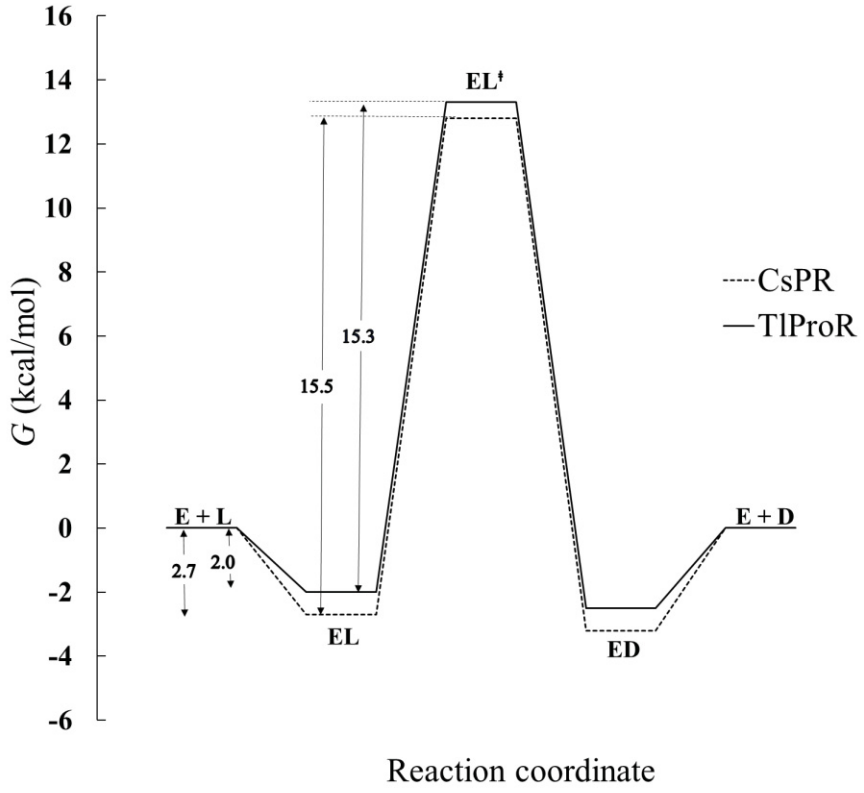

Figure 2.6 Reaction coordinate diagram for reactions catalysed by *Cs*PR and *Tl*PR with L- and D-proline as substrates. The free energy profiles were generated using energy values from **Table 2.3**, where E is the enzyme, L is L-proline, D is D-proline, EL and ED are enzyme-substrate complexes with the corresponding substrates and $EL^{‡}$ is the enzyme-substrate complex in the transition state. All energies were calculated at 25 °C and the standard state is 1 M for all species.

Table 2.3 Change in enthalpy ($\Delta H^{\ddagger}$), entropy ($\Delta S^{\ddagger}$), and Gibbs free energy ($\Delta G^{\ddagger}$) of activation and free energy (ΔG_s) of substrate binding of *Cs*PR and *Tl*PR catalysis

	***Cs*PR**		***Tl*PR**	
	L-proline	**D-proline**	**L-proline**	**D-proline**
$\Delta H^{\ddagger}$ (kcal/mol)	14.7 ± 0.1	12.8 ± 0.2	14.05 ± 0.12	13.5 ± 0.4
$\Delta S^{\ddagger}$ (kcal/mol·K)	−0.0029 ± 0.0003	−0.010 ± 0.001	−0.0041 ± 0.0003	−0.0073 ± 0.0002
$\Delta G^{\ddagger}$ (kcal/mol)*	15.5 ± 2.9	15.8 ± 3.0	15.3 ± 1.9	15.7 ± 2.0
ΔH_s (kcal/mol)	−15.7 ± 0.2	−16.0 ± 0.2	−15.3 ± 0.4	−13.5 ± 0.09
ΔS_s (kcal/mol·K)	−0.041 ± 0.004	−0.040 ± 0.009	−0.041 ± 0.002	−0.033 ± 0.007
ΔG_s (kcal/mol)*	−2.7 ± 0.2	−3.2 ± 0.5	−2.0 ± 0.3	−2.51 ± 0.09

*All values were calculated at T = 25 °C.

*Cs*PR, suggesting that during the process of evolution, some amount of activity was lost, such that the mesophilic counterpart is slower in catalysing the reaction. But this loss in activity in *Cs*PR is compensated by the increased affinity of *Cs*PR for both L- and D-proline to *Cs*PR so that its overall efficiency (k_{cat}/K_m) is similar to that of *Tl*PR (**Table 2.1** & **2.2**). Hence, *Tl*PR and *Cs*PR are equally good at catalysing the racemisation of proline.

The turnover of proline catalysed by both *Cs*PR and *Tl*PR is temperature dependent in accord with the Eyring & Polanyi equation. The major contribution to the free energy of activation ($\Delta G^{\ddagger}$) for both of these enzymes arises from enthalpic contributions ($\Delta H^{\ddagger}$), with only a minor contribution from the change in the entropy of activation ($\Delta S^{\ddagger}$). Reactions catalysed by thermophilic enzymes have been observed to have higher $\Delta G^{\ddagger}$ values relative to their mesophilic counterparts at the same temperatures (Jaenicke *et al.*, 1996; Beadle *et al.*, 1999). However, the above results reveal that the mesophilic and thermophilic variants of PR do not show such a difference in $\Delta G^{\ddagger}$ values (**Table 2.3**).

Studies have revealed that the increased $\Delta G^{\ddagger}$ values of thermophilic enzymes relative to mesophilic enzymes are attributed to the rigidity of the proteins adapted to higher temperatures as opposed to those adapted to lower temperatures (Tsai *et al.*, 1999; Kumar *et al.*, 2000). The active site of PR, as understood from the crystal structure of *Tc*PR (a mesophilic PR), is restricted to any significant movement (Buschiazzo *et al.,* 2011). This suggests that the active site of PR is rigid, irrespective of its temperature adaptation and thus, to an extent, explains the similarity in $\Delta G^{\ddagger}$ values observed for the racemisation of proline catalysed by both *Cs*PR and *Tl*PR.

The change in free energy accompanying binding of L-proline to *Cs*PR (ΔG_s) is ~100 cal/mol less than that for the binding of L-proline to *Tl*PR, suggesting that, *Cs*PR is only marginally better at binding L-proline relative to *Tl*PR. We observed that the Michaelis constant (K_m) of *Tl*PR for L-proline is 33.7 ± 2.5 mM, which is in disagreement with the value reported by Watanabe *et al.* (K_m = 1.2 ± 0.01 mM, Watanabe *et al.*, 2015). The catalytic activity (k_{cat}) of *Tl*PR that we measured (k_{cat} = 265.6 ± 15.0 s^{-1}) was also greater than the reported value of 167 ± 10 s^{-1}. Thus, the observed lower affinity is not likely due to misfolding or an aggregation phenomena occuring during enzyme preparation. Since the expected high affinity of *Tl*PR for L-proline was not observed, making this enzyme no longer a candidate for studies with weak binding alternative substrates (e.g., pipecolic acid, NEA, or NMA). Therefore, subsequent experiments were carried out using *Cs*PR as the model enzyme.

The rate of deprotonation of the proline zwitterion in water at pH 8.0 was determined to be 4.5 × 10^{-11} s^{-1} by Williams *et al*., 2003. Considering this value as the non-enzymatic rate of racemisation of proline (k_{non}), the rate enhancement (k_{cat}/k_{non}) is calculated to be 3.2 × 10^{11}. This value is intermediate when compared to other enzymes for which the rate enhancements have been determined (**Figure 2.7**, Wolfenden & Snider, 2001) Combining the value of k_{non} with the catalytic efficiency of the racemisation of L-proline by *Cs*PR (k_{cat}/K_m), the apparent binding constant of the altered substrate in the transition state (K_{tx}) may be calculated using **equation. 2.4** to be 5.3 × 10^{-15} M at 37 °C.

$$K_{tx} = \frac{k_{non}}{(k_{cat}/K_m)} \tag{2.4}$$

This corresponds to ~19.4 kcal/mol of transition state stabilisation free energy contributed by *Cs*PR. Thus, PR is a highly proficient enzyme, with an enzyme proficiency (reciprocal of K_{tx}) of 1.9 × 10^{-14} M^{-1} and falls in between chorismate

mutase (4.2×10^{-10} M^{-1}, Radzicka & Wolfenden, 1995) and ketosteroid isomerase (1.8×10^{-15} M^{-1}, Radzicka & Wolfenden, 1995) on the scale of enzyme proficiencies described by Wolfenden (**Figure 2.8**, Wolfenden & Snider, 2001).

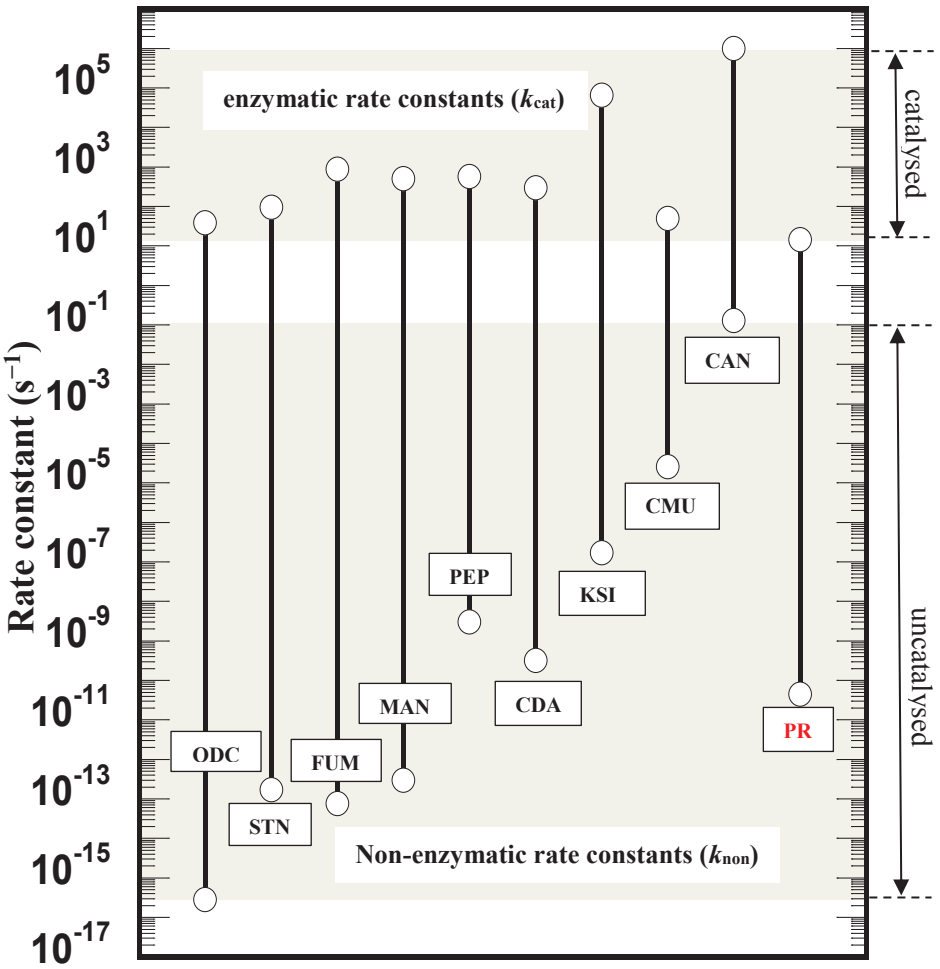

Figure 2.7 Logarithmic scale of enzymatic (k_{cat}) and non-enzymatic (k_{non}) rate constants for some representative reactions. The length of each vertical line corresponds to the rate enhancement (k_{cat}/k_{non}) by OMP-decarboxylase (ODC)[a], staphylococcal nuclease (STN)[a], fumarase (FUM)[b], mandelate racemase (MAN)[c], carboxypeptidase A (PEP)[a], cytidine deaminase (CDA)[a], ketosteroid isomerase (KSI)[a], chorismate mutase (CMU)[a] and proline racemase (PR, in red).
a Radzicka & Wolfenden, 1995
b Bearne & Wolfenden, 1995
c Bearne & Wolfenden, 1997

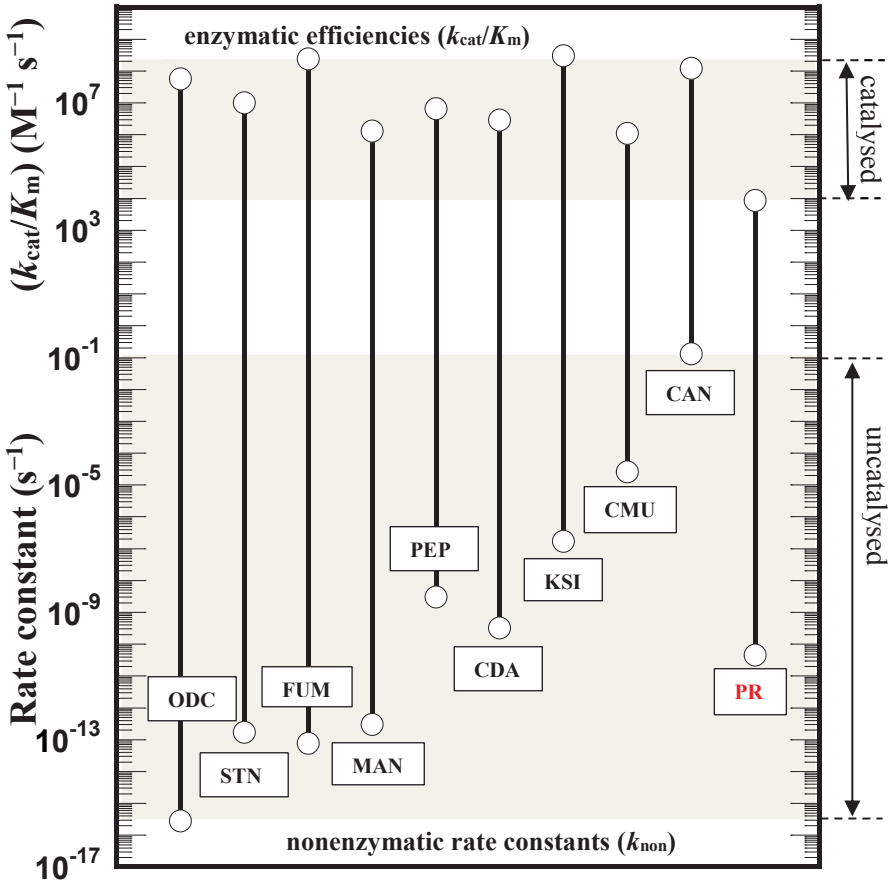

Figure 2.8 Logarithmic scale of enzyme efficiencies (k_{cat}/K_m) and non-enzymatic (k_{non}) rate constants for some representative reactions. The length of the vertical line corresponds to the enzyme proficiency (reciprocal of K_{tx}) of the enzymes (as identified in **Figure 2.7**).

CHAPTER 3

INHIBITION AND KINETICS OF *Cs*PR WITH THE SUBSTRATE ANALOGUE, *N*-ETHYL-L-ALANINE

3.1 INTRODUCTION

*Cs*PR is a highly substrate-specific enzyme with only a limited number of substrates known, of which L- (K_m = 9.5 ± 0.5 mM) and D-proline (K_m = 4.1 ± 0.6 mM) bind with the highest affinities. The rates of *Cs*PR-catalysed racemisation of hydroxy-L-proline and allohydroxy-D-proline are 2% and 5%, respectively, relative to L-proline. Pyrrole-2-carboxylic acid, the *aci*-carboxylate intermediate analogue, inhibits the *Cs*PR-catalysed racemisation of L-proline with a binding constant (K_i) of 0.7 mM. Other inhibitors of *Cs*PR catalysis identified include 2-thiophene carboxylic acid an *aci*-carboxylate intermediate analogue with a sulphur in the position of the nitrogen, which showed 73% inhibition proline concentration of (5.7×10^{-2} M). Maleic acid (93% inhibition), sarcosine (54% inhibition) and pipecolic acid (18% inhibition) are the other inhibitors that were tested for inhibition of *Cs*PR-catalysed racemisation of L-proline by Cardinale & Abeles, 1968 (proline concentration of 5.7×10^{-2} M).

Harty *et al.* designed substrate-product analogues as inhibitors of *Cs*PR catalysis including a bicyclic substrate-product analogue of proline, 7-azabicyclo[2.2.1]heptan-7-ium-1-carboxylate, that showed only 29% inhibition at 142.5 mM (proline concentration of 5.0 mM, Harty *et al.*, 2014). Another such inhibitor was a more flexible bicyclic substrate-product analogue tetrahydro-1H-pyrrolizine-7a(5H)-carboxylate, which was a non-competitive inhibitor of *Cs*PR catalysis with a K_i of 111 mM (proline concentration of 8.0 mM, Harty *et al.*, 2014). The weak binding of these

bicyclic analogues was attributed to the active site being inflexible and not tolerant to increased bulk.

Among the aforementioned substrates and inhibitors of *Cs*PR, it is important to note that, most of these compounds contain an intact-ring structure as in the structure of proline itself (**Figure 3.1**). The question that arises from this observation is: What effect does "breaking" the ring structure have on *Cs*PR catalysis? To understand the importance of this ring structure in *Cs*PR catalysis, we designed a compound that lacks the intact-ring by "breaking" a C-C bond in the ring of proline, i.e., *N*-ethylalanine. Loss of the ring structure would introduce increased entropy, due to the ethyl and methyl groups being free to rotate around their corresponding bonds to the amine group. In this chapter, the kinetic parameters of inhibition of *Cs*PR-catalysed racemisation of L-proline by *N*-ethyl-L-alanine are examined.

3.2 MATERIALS AND METHODS

3.2.1 General

L-Proline and all other reagents, unless mentioned otherwise, were purchased from Sigma-Aldrich Canada Ltd. (Oakville, ON, Canada). Circular dichroism (CD) experiments were conducted using a JASCO J-810 spectropolarimeter (Jasco Inc., Easton, MD), with a temperature-controlled jacketed cell holder. NMR analyses were conducted at the Nuclear Magnetic Resonance Research Resource (NMR-3) facility, Dalhousie University, Halifax, NS, Canada, using either a Brüker AV-300 spectrometer or a Brüker AV-500 spectrometer. Chemical shifts reported (δ) for ^{1}H and ^{13}C experiments are in ppm with respect to TMS at 0 ppm. The deuterium signal

Substrates

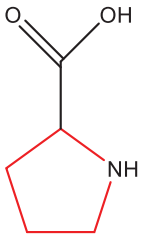

proline[a]

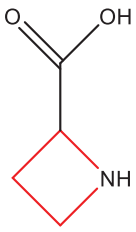

azetidine-2-carboxylic acid[b]

Inhibitors

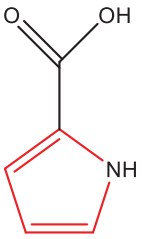

pyrrole-2-carboxylic acid[a]

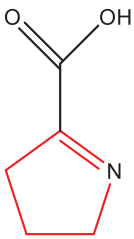

Δ-1-pyrroline-2-carboxylic acid[d]

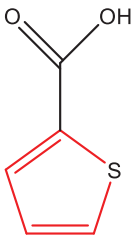

thiophene-2-carboxylic acid[a]

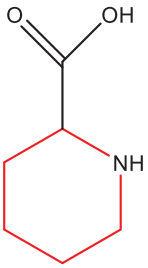

pipecolic acid[a]

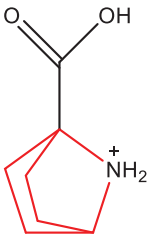

7-azabicyclo[2.2.1]heptan-7-ium-1-carboxylate[c]

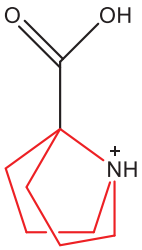

tetrahydro-1H-pyrrolizine-7a(5H)-carboxylate[c]

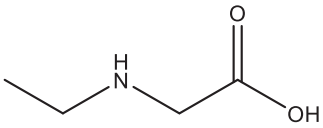

sarcosine[a]

Figure 3.1 Substrates and inhibitors of *Cs*PR catalysis.

a. Cardinale & Abeles, 1968
b. Conti *et al.,* 2011
c. Harty *et al.,* 2014
d. Keenan & Alworth, 1974

from the deuterated solvent was used to lock the spectrophotometer frequency for ^{1}H and ^{13}C NMR. High resolution electrospray ionization (ESI) mass spectra (HRMS) were collected using a Brüker microTOF Focus orthogonal ESI-TOF mass spectrometer instrument operating in the positive ion mode. High performance liquid chromatography with optical rotation detection (HPLC-OR) was conducted using a Waters 510 solvent delivery system (Waters, Milford, MA, USA) and a Jasco OR-4090 optical rotation detector (Jasco Inc., Easton, MD).

3.2.2 Synthesis of *N*-ethyl-L-alanine

N-Ethyl-L-alanine (L-NEA) was prepared by a two-step synthesis as described by Stodulski and Mlynarski, 2008. To a solution of Z-L-alanine i.e., cbz-alanine (9.99 mmol, 2.23 g) in 50 mL of tetrahydofuran (THF), ethyliodide (22.03 mmol, 6.7 mL) and sodium hydride (0.05 mmol, 1.2 g) were added separately in that order at 0 °C under argon with constant stirring. The mixture was then brought to room temperature and refluxed at 60 °C for 12 - 48 h. After completion of the reaction, the mixture was cooled to 0 °C and quenched with water followed by washes with ethyl acetate (3 × 100 mL). The aqueous layer was acidified to pH 4.0 with citric acid (0.5 mM) and further extracted with ethyl acetate (3 × 100 mL). The organic layer was washed with brine solution, dried under sodium sulphate and the ethyl acetate was removed under pressure to obtain *N*-cbz-*N*-ethyl-L-alanine which was further purified using solid phase extraction (SPE) column chromatography (Strata C18-E, 55 µM, 70 Å, Phenomenex, Inc.) with ethylacetate:hexanes (1:1) as the solvent.

The purified *N*-cbz-*N*-ethyl-L-alanine was then dissolved in a mixture of ethanol and water (1:1, 20 mL) and 10% palladium on charcoal (2.5 g) was added with constant stirring. The reaction was allowed to progress for 48 h under hydrogen (balloon). The mixture was then filtered using Celite 545 (Fisher Scientific company,

Fairlawn, NJ, USA) and lyophilised to yield L-NEA as a white solid (0.443 g, 34%): mp 70-72 °C; ^{1}H NMR (D_2O, 300 MHz): δ 1.16 (t, J = 7.2 Hz, 3H, CH_3), 1.34 (d, J = 7.0 Hz, 3H, CH_3), 2.95 (q, J = 7.2 Hz, 2H, CH_2), 3.52 (q, J = 7.0 Hz, 1H, CH(NH)CH_3); ^{13}C NMR (D_2O, 125 MHz ^{1}H-decoupled): δ 10.81 (CH$_3$), 15.14 (CH$_3$), 41.59 (CH$_2$), 57.49 (CH(NH)CH_3), 175.0552 (COOH). HRMS (ESI$^+$) m/z calculated for $C_5H_{11}NO_2$ [M+Na]$^+$: 140.0790, found 140.0677.

3.2.3 Molar ellipticity of *N*-ethyl-L-alanine

To determine the molar ellipticity $[\theta]_\lambda$ of L-NEA, various concentrations of L-NEA (2, 4, 6, 8 and 10 mM) were prepared in Tris-HCl buffer (50 mM, pH 8.0) containing EDTA (8 mM) and the ellipticity was measured at wavelengths from 190−260 nm. Similarly, the ellipticity of only Tris-HCl buffer (50 mM, pH 8.0) containing EDTA (8 mM) was measured over the same wavelengths. These spectra were measured in triplicate and then averaged. The average buffer spectrum was the subtracted from the averaged L-NEA spectrum. The wavelength corresponding to maximum ellipticity (λ_{max}) at which the voltage was low enough to permit increasing the concentration of L-NEA or other reaction components, was chosen and the ellipticities at this wavelength were plotted as a function of concentration to determine $[\theta]_\lambda$.

3.2.4 Circular dichroism spectroscopy-based *Cs*PR assay of L-NEA binding

*Cs*PR activity was measured by following the change in ellipticity of L-proline with time using a CD-based assay at 220 nm with a 0.1-cm light path. The IC_{50} value for inhibition of *Cs*PR by L-NEA was determined by measuring the activity in the presence of varying concentrations of L-NEA at 37 °C and 15 °C. The reaction was

conducted in Tris-HCl buffer (50 mM, pH 8.0) containing EDTA (8 mM) with L-proline as the substrate (9.5 mM final concentration) and L-NEA as inhibitor (0-200 mM final concentration). This mixture was pre-incubated at the indicated temperatures for 5 min followed by the initiation of the reaction by the addition of *Cs*PR (280 nM final concentration), to yield a final reaction volume of 500 µL. A 300-µL aliquot of the mixture was then transferred to a quartz cuvette (0.1-cm light path) to measure the change in ellipticity with time (over 5 min). These changes in ellipticity were used to calculate velocities using the molar ellipticity values ($[\theta]_{220}$) as 6800 (± 54) and −6800 (± 54) deg mol^{-1} cm^2 of L- and D-proline, respectively (Harty *et al.*, 2014).

3.2.5 Circular dichroism spectroscopy-based *Cs*PR assay with L-NEA as the substrate

*Cs*PR activity was monitored by following the change in ellipticity of L-NEA with time using a CD-based assay. The reaction mixture consisting of Tris-HCl buffer (50 mM, pH 8.0) containing EDTA (8 mM) and *N*-ethyl-L-alanine (200 mM final concentration) as substrate was pre-incubated at 15 °C for 5 min. The reaction was then initiated by the addition of *Cs*PR (2.8 µM final concentration) as described previously for the IC_{50} determination followed by measurement of the change in ellipticity over a period of 48 h. To ensure that there was active enzyme in the reaction mixture, *Cs*PR was added at different time intervals. The changes in ellipticity were then plotted as a function of time.

3.2.6 *Cs*PR assay using HPLC-OR detection

The turnover of the optically active L-NEA by *Cs*PR was analysed using an HPLC-based assay with optical rotation (OR) detection. The reaction mixture

consisting of assay buffer [Tris-HCl buffer (50 mM, pH 8.0) containing EDTA (8 mM)] and L-NEA as the substrate (200 mM final concentration) was pre-incubated at 15 °C for 5 min and the reaction was initiated by addition of *Cs*PR (2.8 μM final concentration). The consumption of L-NEA in the reaction was followed by injecting 50-μL aliquots of the reaction mixture, at 30 min intervals for a period of 9 h, into a reversed phase-HPLC system (Restek Ultra IBD 100A, 250 × 4.6 mm, 5μm, Chromatographic Specialties Inc.) with sodium acetate (50 mM, pH 4.2):acetonitrile (18:7) as mobile phase. The flow rate was 1 mL/min. Two control experiments were set up, with one containing only *Cs*PR (2.8 μM final concentration) and the other, only L-NEA (200 mM final concentration) in assay buffer with all other assay conditions identical. The peak intensities from these experiments were then converted to concentrations of L-NEA using the slope from a standard curve determined as detailed in **section 3.2.7**.

3.2.7 Data analysis

The V_{max} and K_m values for *Cs*PR assays were calculated by fitting **equation 3.1** to the initial velocities (v_i) (Michaelis and Menten, 1913) using non-linear regression analysis and KaleidaGraph v. 4.03 from Synergy software (Reading, PA). The k_{cat} values were then determined by dividing V_{max} values by the concentration of the enzyme. All kinetic parameters were determined in triplicate and the averages with standard deviations from the mean are reported. IC_{50} values were determined by fitting **equation 3.2**, where n is the Hill number, to the relative initial velocities where v_i is the initial velocity in the presence of inhibitor and v_o is the initial velocity in the absence of inhibition. The molar ellipticity ($[\theta]_\lambda$) of L-NEA at a given wavelength (λ) was calculated using **equation 3.3**.

$$v_i = \frac{V_{max}[S]}{K_m + [S]} \tag{3.1}$$

$$\frac{v_i}{v_o} = \frac{{IC_{50}}^n}{{IC_{50}}^n + [I]^n} \tag{3.2}$$

$$[\theta]_\lambda = \frac{100 \times \theta}{c\ (\text{mM}) \times l\ (\text{cm})} \tag{3.3}$$

3.3 RESULTS

3.3.1 Product analysis

The structure of the final product, L-NEA, was confirmed using ^{1}H and ^{13}C NMR experiments (**Figures 3.2** and **3.3**), and the chemical shifts were in accord with those reported by Stodulski and Mlynarski, 2008. The exact mass of the L-NEA as a sodium ion adduct was confirmed to be 140.0677, by mass spectrometry experiments (**Figure 3.4**). The molar ellipticity of L-NEA was determined using the slopes from the calibration curve (**Figure 3.6**) and was found to be 6264.77 (± 30.32) deg mol^{-1} cm^2. The optimal wavelength for CD assays was chosen to be 220 nm (**Figure 3.5**).

3.3.2 Inhibition of *Cs*PR by *N*-ethyl-L-alanine

L-NEA showed no inhibition of *Cs*PR activity at 37 °C (**Figure 3.7 A**). At lower temperatures, one can expect better binding of the ligand to the enzyme due to decreased entropic effects. Indeed, at 15 °C, L-NEA inhibited *Cs*PR activity to ~70% of the full activity at a concentration of 200 mM, but with an $IC_{50} > 200$ mM (**Figure 3.7 B**). Extrapolation of the inhibition data gave $IC_{50} \approx 396.4 \pm 80.7$ mM with $n = 1.2$

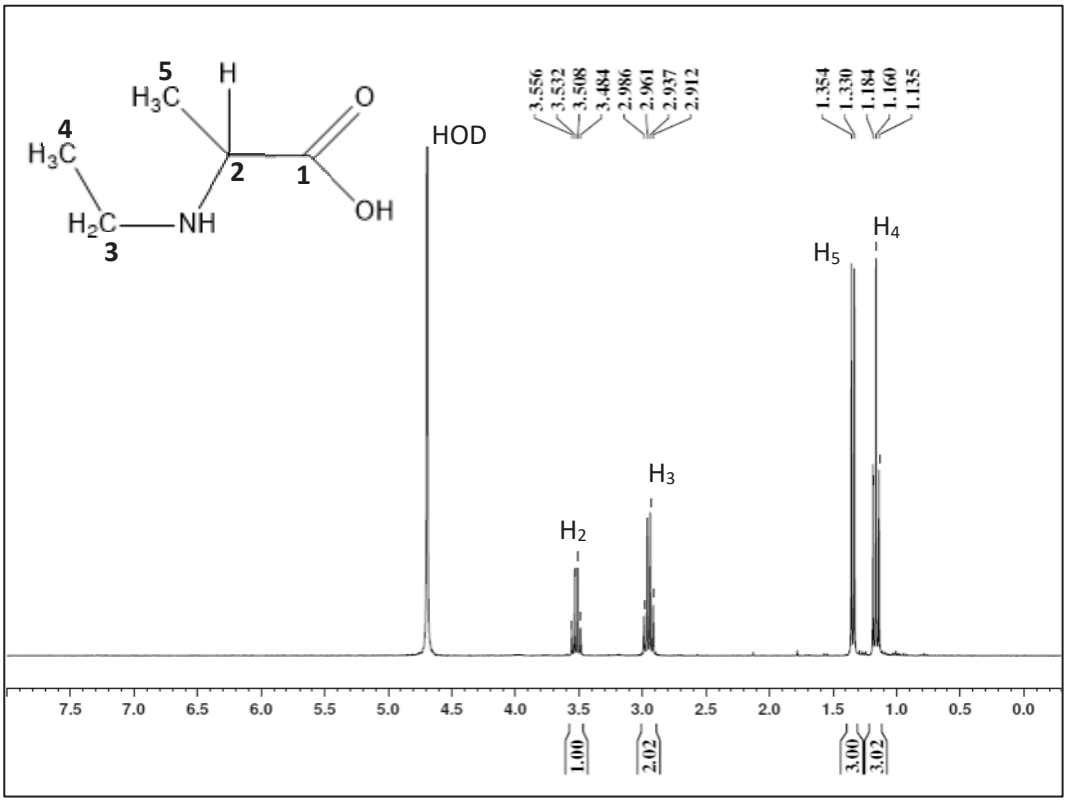

Figure 3.2 ^{1}H NMR spectrum of *N*-ethyl-L-alanine in D_2O. The integrals from each peak are shown below the x-axis. The signal at 4.69 ppm corresponds to the HOD signal. The spectrum was obtained using the 300 MHz Brüker AV-300 specrometer.

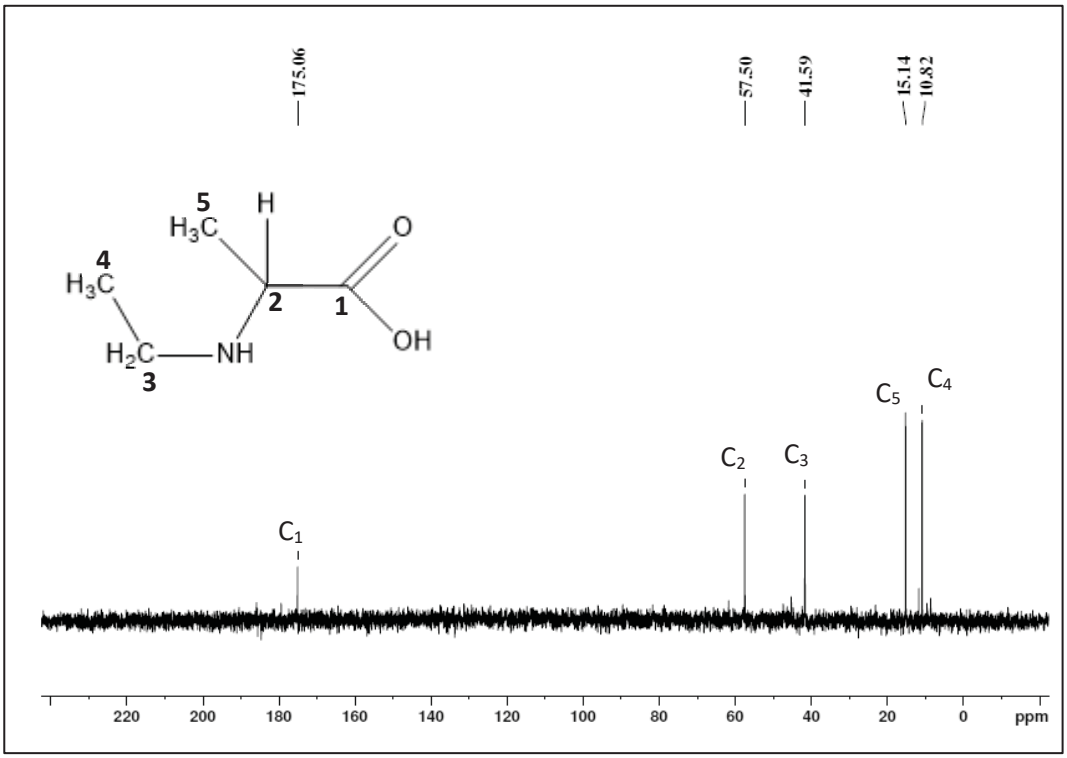

Figure 3.3 ^{13}C NMR (^{1}H-decoupled) spectrum of *N*-ethyl-L-alanine in D_2O. The spectrum was obtained using the 500 MHz Brüker AV-500 specrometer.

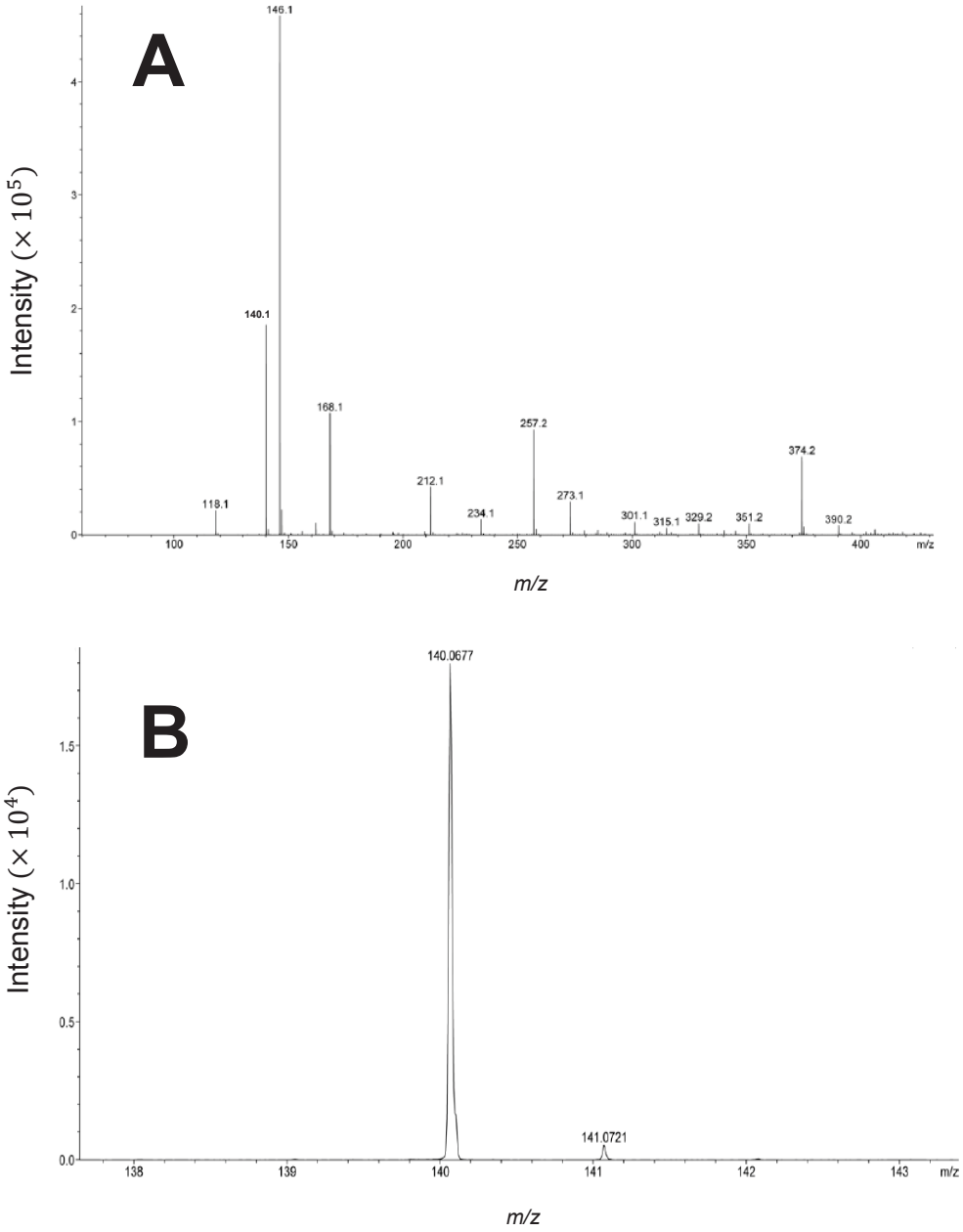

Figure 3.4 Mass spectra of *N*-ethyl-L-alanine. A low resolution spectrum (**A**) and a high resolution spectrum focussing on the expected [L-NEA-Na]$^+$ adduct peak at 140.0677 *m/z* (**B**) which agrees with the expected mass of 140.0790 *m/z* for the [L-NEA-Na]$^+$ adduct.

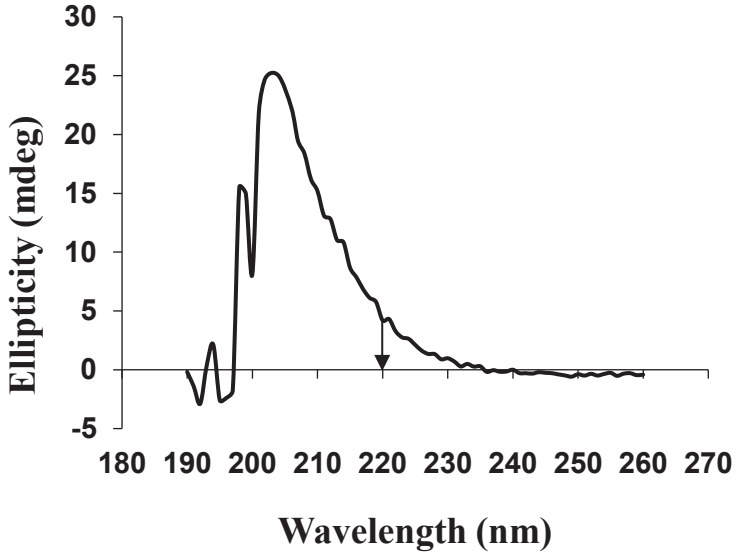

Figure 3.5 Circular dichroism spectrum of L-NEA. The spectrum obtained is at 10 mM L-NEA concentration with the optimal wavelength for assays chosen to be 220 nm indicated by the downward arrow.

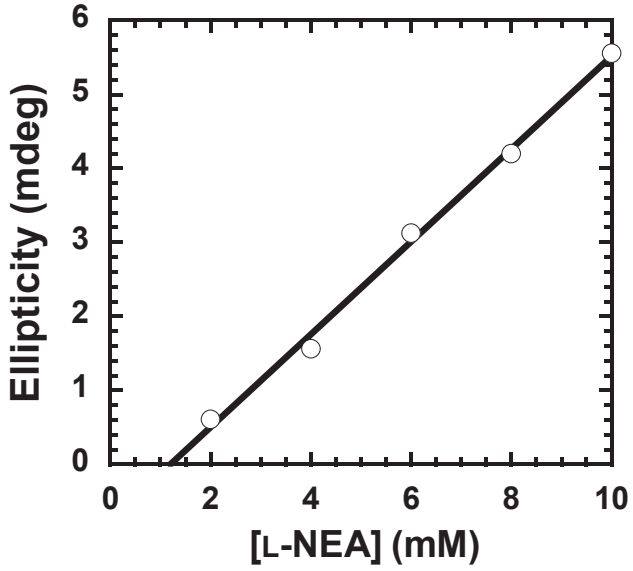

Figure 3.6 Standard curve of L-NEA to determine its molar ellipticity. The ellipticities (θ) at 220 nm were determined from the CD spectra. The molar ellipticity ($[\theta]_{220}$) was calculated from the slope of the regression line: $\theta = 0.62647\ (\pm 0.00303)[\text{L-NEA}] + 0.74780\ (\pm 0.00373)$. All experiments were conducted at 15 °C.

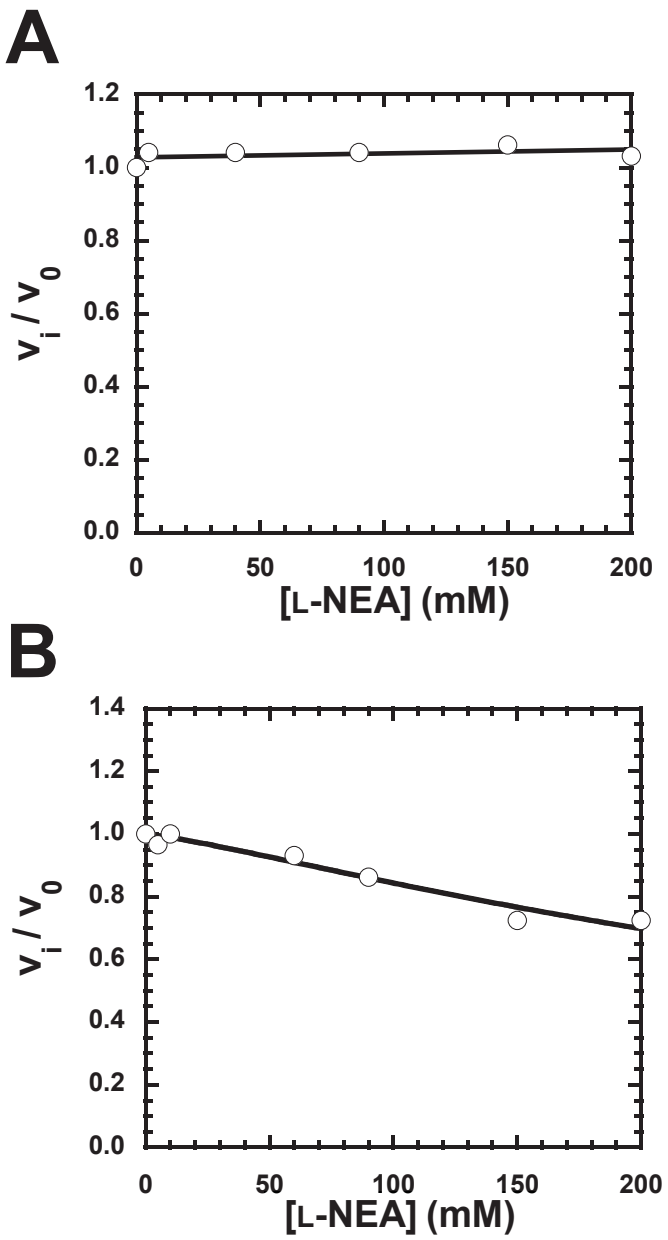

Figure 3.7 IC_{50} curves for the inhibition of *Cs*PR-catalysed racemisation of L-proline by L-NEA at 37 °C (A) and 15 °C (B). No inhibition was observed at 37 °C, however weak inhibition was observed at 15 °C and the IC_{50} value was obtained by extrapolation to be 396.4 ± 80.7 with n = 1.2 ± 0.2. All experiments were conducted at 15 °C.

± 0.2. Thus, it can be concluded that *Cs*PR binds L-NEA, but with a very low affinity (< 20-fold) relative to L-proline (K_m = 9.5 mM).

3.3.3 *N*-Ethyl-L-alanine as a substrate of *Cs*PR

Since it was established that *Cs*PR binds L-NEA, a *Cs*PR assay was conducted to determine if L-NEA could act as a substrate. The CD-based assay with L-NEA, followed over a period of 48 h, showed an overall change in ellipticity (**Figure 3.8**). The ellipticity was also monitored for *Cs*PR and L-NEA individually. While the ellipticity for these two components did not change, the ellipticity did drop substantially when enzyme and L-NEA were present together. This observation suggests that L-NEA serves as a substrate for *Cs*PR.

In the HPLC-OR assay, a decrease in the peak intensity corresponding to L-NEA by ~40% was observed indicating turnover of L-NEA over a period of 9 h (**Figure 3.9**). The efficiency of the enzyme (k_{cat}/K_m) with L-NEA as a substrate was estimated using **equation 3.1** and assuming [S] << K_m. The value of (k_{cat}/K_m) was found to be 0.0018 $mM^{-1}s^{-1}$, dramatically (~4,500-fold) less than that for *Cs*PR-catalysed racemisation of L-proline (8.2 $mM^{-1}s^{-1}$).

3.4 DISCUSSION

"Breaking" a C-C bond in the L-proline ring to form L-NEA introduces additional entropy into the system due to free to rotation of the methyl and ethyl groups generated relative to the compact, closed ring of L-proline. The entropic contribution to the free energy of a reaction is temperature dependent ($T\Delta S$), and it is expected to decrease with a decrease in temperature. This effect was observed when L-NEA was tested as an inhibitor for *Cs*PR catalysis at two temperatures, 15 and 37 °

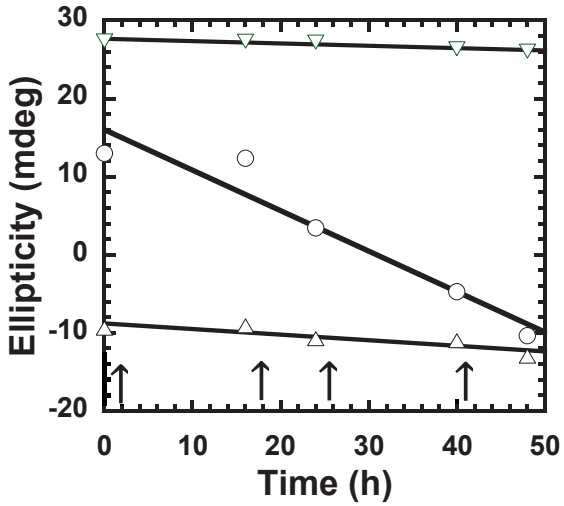

Figure 3.8 Change in ellipticity of L-NEA in a *Cs*PR-catalysed reaction. The reaction was followed over a period of 48 h (○) and two control experiments- only L-NEA (▽) and only *Cs*PR (△) are also plotted. All experiments were conducted at 15 °C. The arrows (↑) indicate the addition of fresh enzyme (2.8 μM).

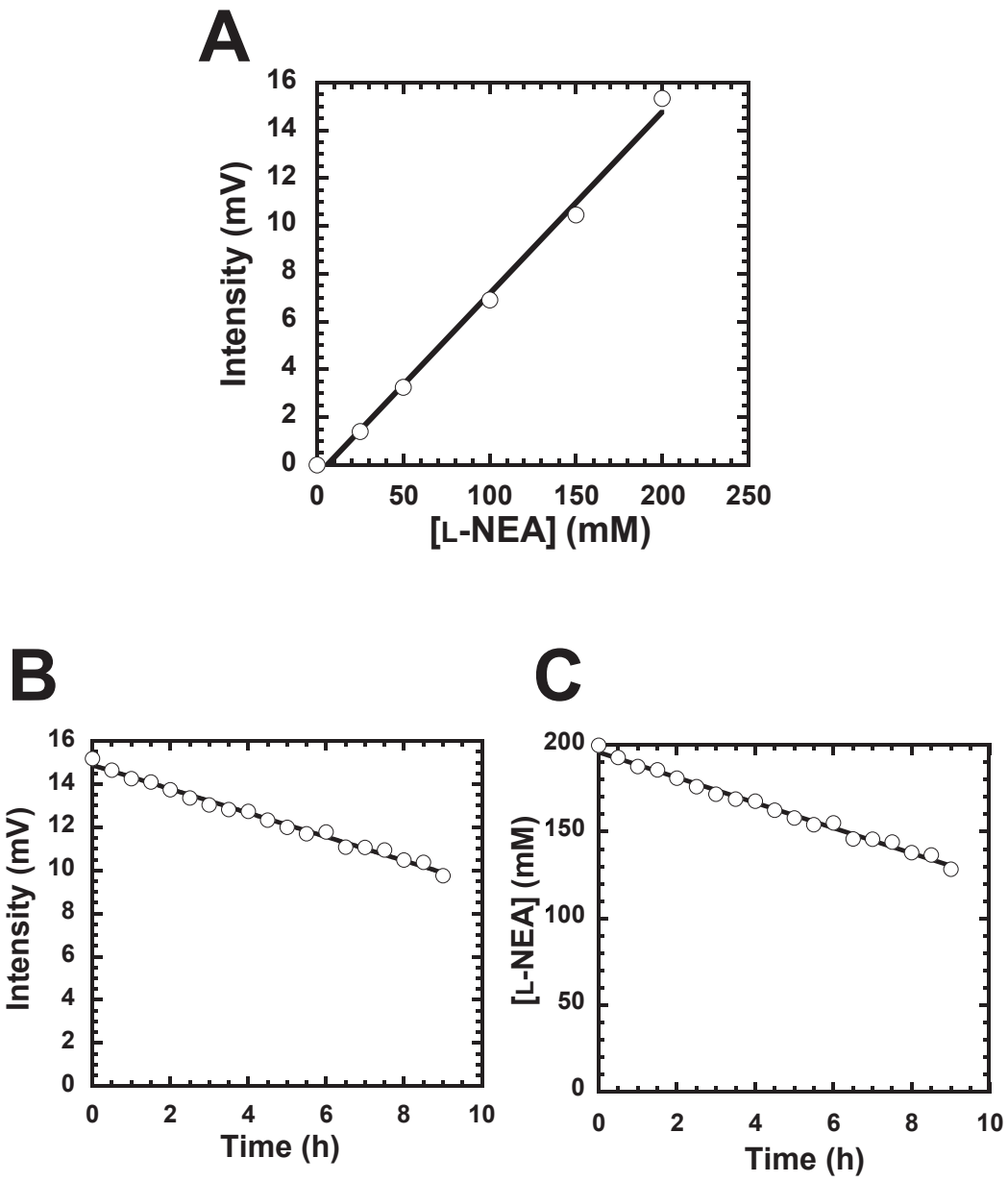

Figure 3.9 HPLC-OR assay for analysing L-NEA turnover in the reaction catalysed by *Cs*PR. A standard curve for intensities corresponding to different concentrations of L-NEA (**A**) with the linear regression equation: $intensity = 0.0760\ \left(\frac{\text{mV}}{\text{mM}}\right)[\text{L}-\text{NEA}] - 0.4269(\text{mM})$ are shown. The change in intensity of optical rotation of L-NEA with time (**B**) with the linear regression equation: $intensity = -0.5538\ \left(\frac{\text{mV}}{\text{h}}\right)(\text{time}) + 14.8863\ (\text{mV})$ is shown. The change in L-NEA concentration with time (**C**) with the linear regression equation: $[\text{L}-\text{NEA}] = -7.2886\ \left(\frac{\text{mM}}{\text{h}}\right)(\text{time}) - 195.92\ (\text{mM})$. All experiments were conducted at 15 °C.

C. L-NEA failed to inhibit the *Cs*PR-catalysed racemisation of L-proline at 37 °C but exhibited weak inhibition of *Cs*PR catalysis at 15 °C (i.e., IC_{50} value >> 200 mM) (**Figure 3.6**). This study suggested that, though L-NEA is a poor inhibitor of *Cs*PR catalytic activity, it does bind to *Cs*PR, which led us to investigate whether or not L-NEA is a substrate of *Cs*PR.

The *Cs*PR-catalysed racemisation of L-NEA was found to be very slow, with the ellipticity of a reaction solution being reduced over a period of 48 h with several additions of fresh enzyme. HPLC experiments confirmed that this change in ellipticity was due to the racemisation of L-NEA catalysed by *Cs*PR, as a decrease in the concentration of L-NEA was observed over a period of 9 h. The consumption of L-NEA over 9 h in the reaction catalysed by *Cs*PR was quantified by calculating the catalytic efficiency (k_{cat}/K_m) to be 0.0018 $mM^{-1}s^{-1}$. A massive 4,500-fold decrease in catalytic efficiency relative to L-proline racemisation catalysed by *Cs*PR at 15 °C was observed, suggesting that L-NEA is indeed a very poor substrate of *Cs*PR. Such low activity with L-NEA could be due to two reasons: (1) failure of the open-ring analogue to bind with the correct orientation in the active site and/or (2) a lower affinity of the enzyme towards the substrate because of steric effects adversely affecting formation of the enzyme-substrate complex. Since the *Cs*PR-catalysed racemisation of L-NEA is very slow, as suggested by the estimated catalytic efficiency, several practical challenges must be overcome to further analyse the kinetics of this reaction. Some practical limitations include long reaction times that might lead to reduced activity of the enzyme with time. One way to allow the reaction to proceed faster is by increasing the temperature of the reaction solution. But *Cs*PR has poor affinity for NEA, thus increasing the temperature would worsen this binding affinity. The *Cs*PR assays with NEA described in this study were analysed using CD

spectroscopy that limited the working concentration range of NEA to less than 200 mM. This could be overcome by using alternative analytical techniques like HPLC for better kinetic analysis.

Thus, opening the ring-structure of proline, and increasing the entropy of the substrate appears to lead to an overwhelming loss in the activity of *Cs*PR. To address whether or not this effect arises from the steric bulk of NEA, relative to proline, we examined the ability of *Cs*PR to catalyse the racemisation of L-pipecolic acid. This putative substrate is slightly larger than proline with one additional methylene unit but retains the ring structure. The results of this study are presented in the next chapter.

CHAPTER 4

INVESTIGATION OF STERIC EFFECTS ON SUBSTRATE BINDING DURING PROLINE RACEMASE CATALYSIS

4.1 INTRODUCTION

The design of competitive enzyme inhibitors generally involves mimicking the structure of the substrate(s), products(s), transition state, or the intermediate(s) of the reaction being catalysed. The active sites of racemases and epimerases are exceptionally "designed" through evolution so that they can accommodate both stereoisomers, i.e., the substrate and the product. For example, benzilate, a substrate-product analogue of mandelic acid, inhibited mandelate racemase with a K_i value of 0.6 mM (*cf.* K_m = 1.0 mM) (Lietzan *et al.*, 2012; Siddiqi *et al.,* 2005; Maurice and Bearne, 2004) and 2,2-bis(4-isobutylphenyl)propanoyl-CoA, a substrate-product analogue for the enzyme α-methyl CoA inhibited the enzyme with a K_i value of 16.9 μM (K_m = 106 μM) (Pal *et al.*, 2016). Such a strategy design was employed by Harty *et al.* to develop a bicyclic analogue of proline, tetrahydro-1H-pyrrolizine-7a(5H)-carboxylate, as a substrate-product analogue inhibitor of *Cs*PR catalysis but was only a moderate inhibitor (K_i = 111 mM, cf. K_m = 5.7 mM, Harty *et al.*, 2014). This suggests that the active site of *Cs*PR is not as "roomy" as the other enzymes mentioned. Indeed, the X-ray crystal structure of PR from *T. cruzi* (Busciazzo *et al.,* 2006) revealed a sterically constricted active site.

As discussed in the previous chapter, the open-ring analogue of proline, *N*-ethylalanine (NEA), was synthesised to investigate the effect of "breaking" the ring structure of the substrate on *Cs*PR catalysis. Since NEA was a weak inhibitor, a less

bulky inhibitor, *N*-methylalanine (NMA), was chosen for the study. We anticipated that the rigid active site of *Cs*PR would be capable of binding the smaller NMA better than NEA.

Pipecolic acid was reported as a weak inhibitor of *Cs*PR-catalysed racemisation of proline showing 18% inhibition (proline concentration of 5.7×10^{-2} M; Cardinale & Abeles, 1968). This observation raises the question: Is pipecolic acid a substrate of *Cs*PR and can the active site of *Cs*PR accomodate the steric bulk of this compound? This six-membered ring analogue of proline was thus tested for catalytic stereoinversion catalysed by *Cs*PR, which would in turn give insights into steric effects on *Cs*PR-mediated catalysis.

From the other side of the substrate spectrum of *Cs*PR, a four-membered ring analogue of proline, L-azetidine-2-carboxylic acid (ACA) was tested as a substrate for *Cs*PR catalysis. A comparison between the kinetic parameters of the *Cs*PR-catalysed racemisations of these compounds should delineate the steric constraints governing binding of substrate at the active site of *Cs*PR.

4.2 MATERIALS AND METHODS

4.2.1 General

N-Methyl-L-alanine, L-pipecolic acid and D-pipecolic acid were purchased from Tokyo Chemical Industry (TCI) (Cambridge, MA, USA); *N*-methyl-D-alanine from Alfa Aesar (Tewksbury, MA, USA); (*S*)-(−)-L-azetidine-2-carboxylic acid from Synthonix (Wake Forest, NC); L-proline, and all other reagents, unless mentioned

otherwise, were purchased from Sigma-Aldrich Canada Ltd. (Oakville, ON, Canada). Circular dichroism (CD) experiments were conducted using a JASCO J-810 spectropolarimeter (Jasco Inc., Easton, MD), with a temperature-controlled jacketed cell holder.

4.2.2 Molar ellipticity of L- and D-pipecolic acid

The molar ellipticities of L- and D- pipecolic acid were determined as described for L-NEA (**Chapter 3 Section 3.2.3**).

4.2.3 Circular dichroism spectroscopy-based *Cs*PR assay with L- and D-pipecolic acid

*Cs*PR activity was quantified by following the change in ellipticity of L-pipecolic acid with time in a CD-based assay with a 0.1-cm light path at 220 nm. The assay was conducted by pre-incubating the reaction mixture consisting of Tris-HCl buffer (50 mM, pH 8.0) containing EDTA (8 mM) with L-pipecolic acid (50-180 mM final concentration) or D-pipecolic acid (50-160 mM final concentration), at 15 °C for 5 min. The reaction was then initiated by addition of *Cs*PR (150 nM final concentration) such that a final volume of 500 µL was obtained. From this mixture, a 300-µL aliquot was immediately transferred to a 0.1-cm light path quartz cuvette and the change in ellipticity was measured over a period of 5 min. These changes in ellipticity were used to calculate velocities using the molar ellipticity values ($[\theta]_{220}$) of 13866 (± 72) and −13721 (± 86) deg mol^{-1} cm^2 for L- and D-pipecolic acid, respectively (**Figure 4.1**).

4.2.4 Molar ellipticity of *N*-methyl-L-alanine and *N*-methyl-D-alanine

The molar ellipticities of *N*-methyl-L-alanine and *N*-methyl-D-alanine were determined as described for L-NEA (**Chapter 3 Section 3.2.3**).

4.2.5 Inhibition of *Cs*PR catalysis by *N*-methyl-L-alanine

The IC_{50} value for inhibition of *Cs*PR by *N*-methyl-L-alanine was determined by conducting inhibition experiments involving pre-incubation of the assay mixture: Tris-HCl buffer (50 mM, pH 8.0) containing EDTA (8 mM), L-proline (9.5 mM) and *N*-methyl-L-alanine (0-200 mM) at 15 °C for 5 min. *Cs*PR (280 nM final concentration) was added to the mixture (500-µL final volume) to initiate the reaction and a 300-µL aliquot from this mixture was immediately transferred to a 0.1-cm quartz cuvette to follow the change in ellipticity with time over 5 min.

To determine the kinetic parameters for inhibition of *Cs*PR by *N*-methyl-L-alanine, *Cs*PR activity was measured with L-proline as substrate and *N*-methyl-L-alanine as the inhibitor. The assay was conducted at 15 °C and the assay mixture consisted of Tris-HCl buffer (50 mM, pH 8.0) containing EDTA (8 mM), *N*-methyl-L-alanine (0, 16, 32 and 48 mM), and L-proline (0.5-200 mM final concentration). This mixture was pre-incubated at 15 °C for 5 min followed by the addition of *Cs*PR (280 nM final concentration). The change in ellipticity of L-proline was monitored in a 0.1-cm light path quartz cuvette, as described previously.

4.2.6 Circular dichroism spectroscopy-based *Cs*PR assay with *N*-methyl-L-alanine and *N*-methyl-D-alanine

*Cs*PR activity was measured using a CD-based assay by following the change in ellipticity of *N*-methyl-L- and D-alanine at 220 nm with a 0.1-cm light path at 15 °C. The reaction mixture consisted of Tris-HCl buffer (50 mM, pH 8.0) containing EDTA (8 mM) and *N*-methyl-L-alanine (10-250 mM final concentration, L-NMA) or *N*-methyl-D-alanine (50-250 mM final concentration, D-NMA). This reaction mixture was preincubated for 5 min at 15 °C followed by addition of *Cs*PR (150 nM final concentration) to initiate the reaction, yielding a final volume of 500 µL. The change

in ellipticity was then monitored as described previously for *Cs*PR-catalysed racemisation of pipecolic acid. The molar ellipticities of *N*-methyl-L-alanine (7890 ± 30 deg mol^{-1} cm^2) and *N*-methyl-D-alanine (8637 ± 48 deg mol^{-1} cm^2) (**Figure 4.3**) were used to calculate the initial velocities (v_i).

4.2.7 Molar ellipticity of L-azetidine-2-carboxylic acid

The molar ellipticities of L-azetedine-2-carboxylic acid were determined as described for L-NEA (**Chapter 3 Section 3.2.3**).

4.2.8 Circular dichroism-based PR assay with L-azetedine-2-carboxylic acid

To determine the kinetic parameters for the turnover of L-azetedine-2-carboxylic acid (L-ACA) catalysed by *Cs*PR, the change in ellipticity of L-azetedine-2-carboxylic acid was followed using a CD-based assay at 216 nm with a 0.1-cm light path. The assay mixture consisting of Tris-HCl buffer (50 mM, pH 8.0) containing EDTA (8 mM) and L-azetedine-2-carboxylic acid (0.5-120 mM final concentration) was pre-incubated at 15 °C and the reaction was initiated by the addition of *Cs*PR (150 nM final concentration). The change in ellipticity was then measured as mentioned previously for the pipecolic acid assays. The molar ellipticity of L-ACA (15369 ± 70 deg mol^{-1} cm^2) (**Figure 4.7**) was used to calculate the initial velocities (v_i).

4.2.9 Data analysis

The V_{max} and K_m values for *Cs*PR-catalysed racemisation of various L-proline analogues were obtained by fitting **eqn. 4.1** (Michaelis and Menten, 1913) to the initial velocities (v_i) using non-linear regression analysis and KaleidaGraph v. 4.03 from Synergy software (Reading, PA). The k_{cat} values were then determined by

dividing V_{max} values by the concentration of the enzyme. All kinetic parameters were determined in triplicate and the averages with standard deviations from the mean are reported. The IC_{50} values were determined by fitting **eqn. 4.2** to the relative initial velocities (v_i/v_o), where $v_i$is the initial velocity in the presence of inhibitor and $v_o$is the initial velocity in the absence of inhibitor. To determine the mode of inhibition, a double reciprocal plot, $1/v_i$ vs 1/[S], was plotted and the data were fit by **eqn. 4.3.** Linear-mixed inhibition constants (K_i and αK_i) were determined from plots of the apparent K_m/V_{max} values versus inhibitor concentration and the apparent $1/V_{max}$ values versus inhibitor concentration, in accordance with **eqn. 4.4**.

$$v_i = \frac{V_{max}[S]}{K_m + [S]} \tag{4.1}$$

$$\frac{v_i}{v_o} = \frac{{IC_{50}}^n}{{IC_{50}}^n + [I]^n} \tag{4.2}$$

$$\frac{1}{v_i} = \frac{K_m^{app}}{V_{max}^{app}}\frac{1}{[S]} + \frac{1}{V_{max}^{app}} \tag{4.3}$$

$$v_i = \frac{V_{max}^{app}[S]}{K_m\left(1+\frac{[I]}{K_i}\right) + [S]\left(1+\frac{[I]}{\alpha K_i}\right)} \tag{4.4}$$

4.3 RESULTS

4.3.1 Pipecolic acid as a substrate of *Cs*PR

The kinetics of *Cs*PR-catalysed racemisation of the six-membered ring analogues of proline, L- and D-pipecolic acid, revealed that the initial velocities varied linearly with the concentrations of the analogue (**Figure 4.2**), with saturation not being observed in either case over a substrate concentration range of 50 to 200 mM.

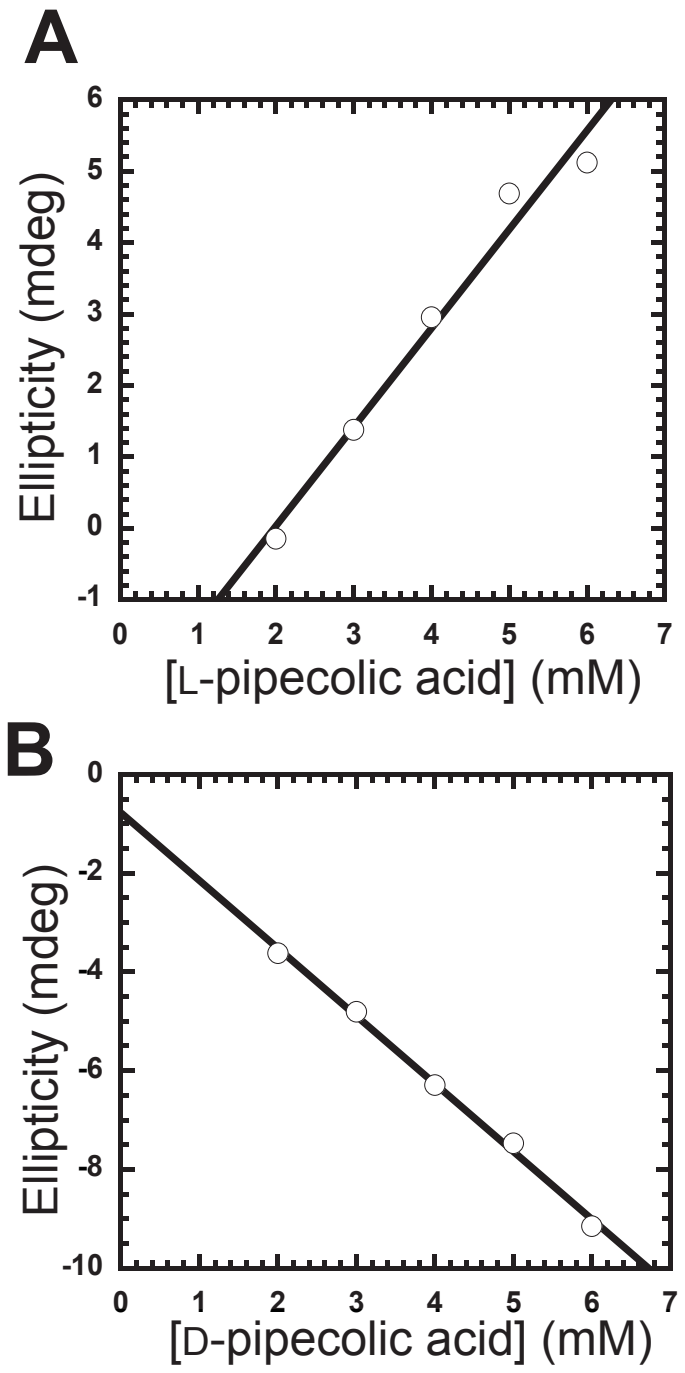

Figure 4.1 Standard curve for determination of the molar ellipticities of L- and D-pipecolic acid. The ellipticities (θ) at 220 nm were determined from the CD spectra. The molar ellipticity ($[\theta]_{220}$) was calculated from the slope of the regression lines: $\theta = 1.38674\ (\pm 0.00593)[\text{L-pipecolic acid}] + 2.74590\ (\pm 0.00732)$ (**A**) and $\theta = -1.37208\ (\pm 0.00624)[\text{D-pipecolic acid}] + 0.77878\ (\pm 0.00201)$ (**B**). All experiments were conducted at 15 °C.

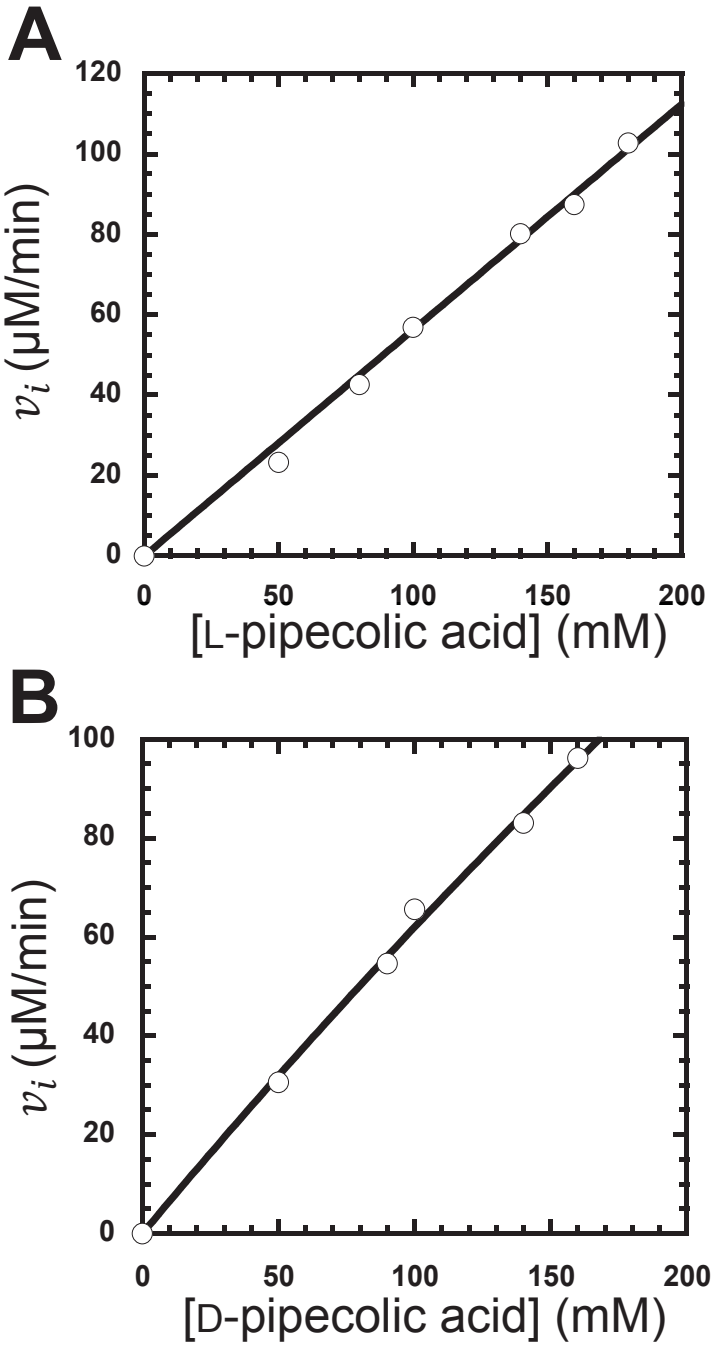

Figure 4.2 Representative Michaelis-Menten plots for *Cs*PR-catalysed racemisation of (A) L-pipecolic acid and (B) D-pipecolic acid. The slopes of the lines yield estimates of k_{cat}/K_m of 0.067 ± 0.005 $mM^{-1}s^{-1}$ **(A)** and 0.073 ± 0.003 $mM^{-1}s^{-1}$ (**B**).

This suggested that a K_m >>200 mM. The k_{cat}/K_m value for the racemisation of L-pipecolic was calculated to be 0.067 ± 0.005 $mM^{-1}s^{-1}$ and that for D-pipecolic acid was 0.073 ± 0.003 $mM^{-1}s^{-1}$, which were significantly reduced in comparison with the corresponding values when L-proline (8.2 ± 0.1 $mM^{-1}s^{-1}$) and D-proline (14.4 ± 0.1 $mM^{-1}s^{-1}$) were employed as substrates. *Cs*PR binds L- and D-pipecolic acid more weakly than it does L- and D- proline, suggesting that the bulky six-membered ring encounters some steric hindrance whilst binding to the active site of *Cs*PR.

4.3.2 *N*-Methylalanine as a substrate of *Cs*PR

The initial velocities for the racemisation of L- and D- NMA catalysed by *Cs*PR follow a linear dependence on the NMA concentration (**Figure 4.4**), with saturation not being attained over a concentration range of 10 to 250 mM, as also observed for the racemisation of pipecolic acid catalysed by *Cs*PR. The catalytic efficiency of the turnover of L- and D- NMA by *Cs*PR was determined to be 0.088 ± 0.006 $mM^{-1}s^{-1}$ and 0.058 ± 0.002 $mM^{-1}s^{-1}$, respectively, suggesting a ~100-fold decrease in comparison to the corresponding value for racemisation of L-proline (8.2 ± 0.1 $mM^{-1}s^{-1}$) and ~200-fold decrease in efficiency relative to that of D-proline (14.4 ± 0.1 $mM^{-1}s^{-1}$). Interestingly, NMA and pipecolic acid exhibited no substantial difference in their catalytic efficiencies, and both substrates were bound by *Cs*PR with lower affinity than observed for proline.

4.3.3 *N*-Methylalanine as an inhibitor of *Cs*PR

Preliminary inhibition studies on the *Cs*PR-catalysed racemisation of L-proline with L-NMA as an inhibitor showed that l-NMA inhibited *Cs*PR with an IC_{50} value of 32.3 ± 1.2 mM (**Figure 4.5**). Surprisingly, when L-NMA was the substrate, the

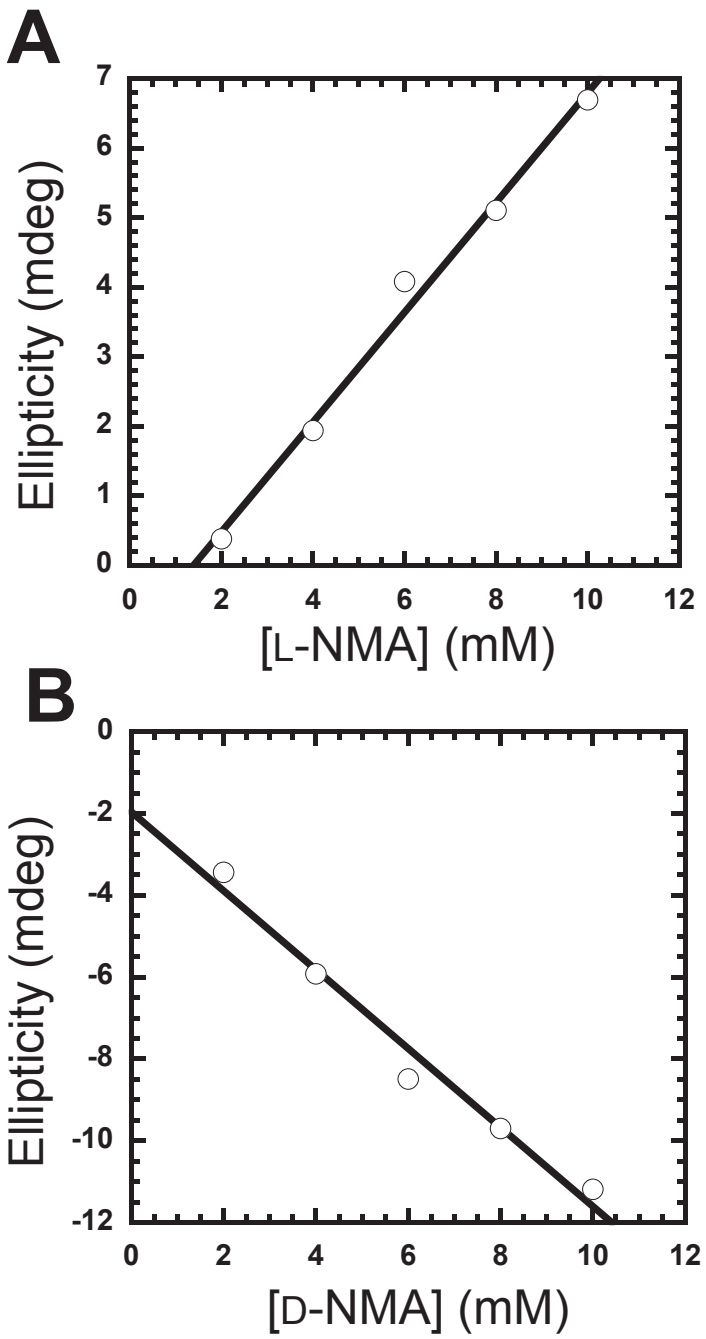

Figure 4.3 Standard curve of L-NMA to determine its molar ellipticity. The ellipticities (θ) at 220 nm were determined from the CD spectra. The molar ellipticity ($[\theta]_{220}$) was calculated from the slope of the regression line: $\theta = 0.78904\ (\pm 0.00297)[\text{L-NMA}] + 1.09343\ (\pm 0.00580)$ (**A**) and $\theta = -0.86369\ (\pm 0.00476)[\text{D-NMA}] + 1.96228\ (\pm 0.00312)$ (**B**). All experiments were conducted at 15 °C.

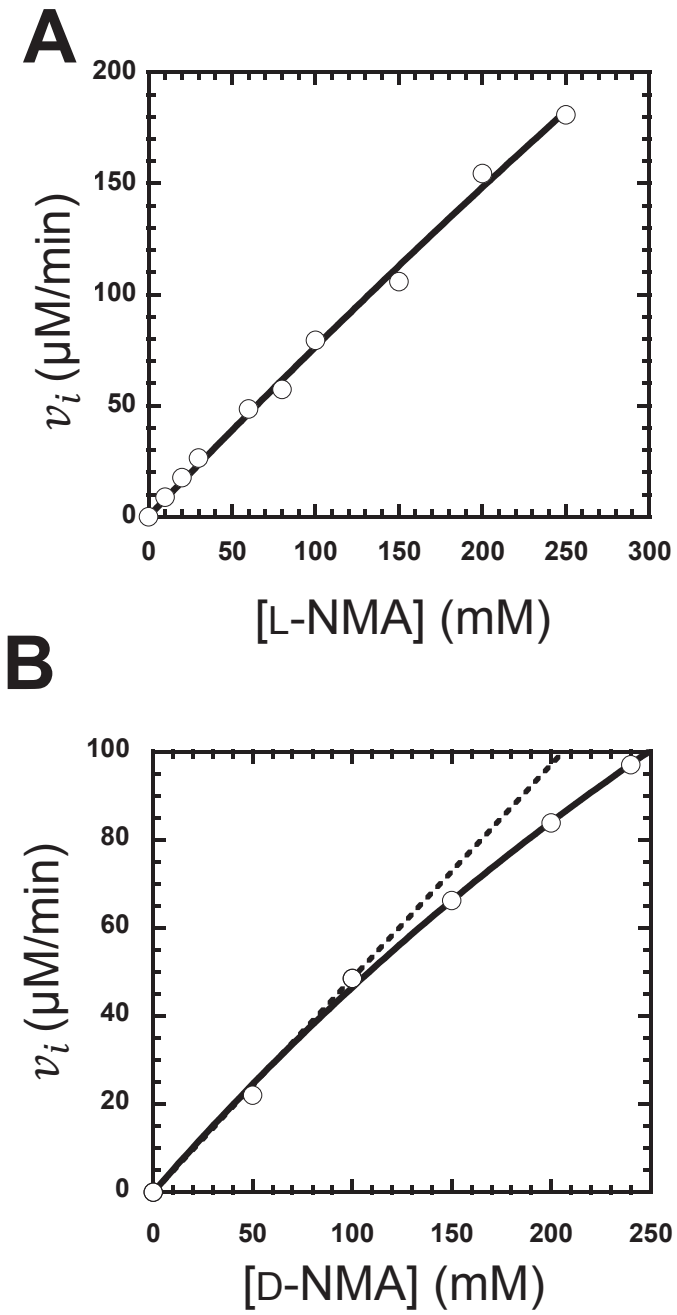

Figure 4.4 Representative Michaelis-Menten plots for *Cs*PR-catalysed racemisation of (A) L-NMA and (B) D-NMA. In plot (**B**), a slight curvature in the data fit to **eqn. 4.1** is observed, thus a dotted regression line is extrapolated through the linear region of the curve defined by the equation: $v_i = 0.04853$ [D-NMA]. The slopes of the lines yield estimates of k_{cat}/K_m of 0.088 ± 0.006 $mM^{-1}s^{-1}$ **(A)** and 0.058 ± 0.002 $mM^{-1}s^{-1}$ (**B**).

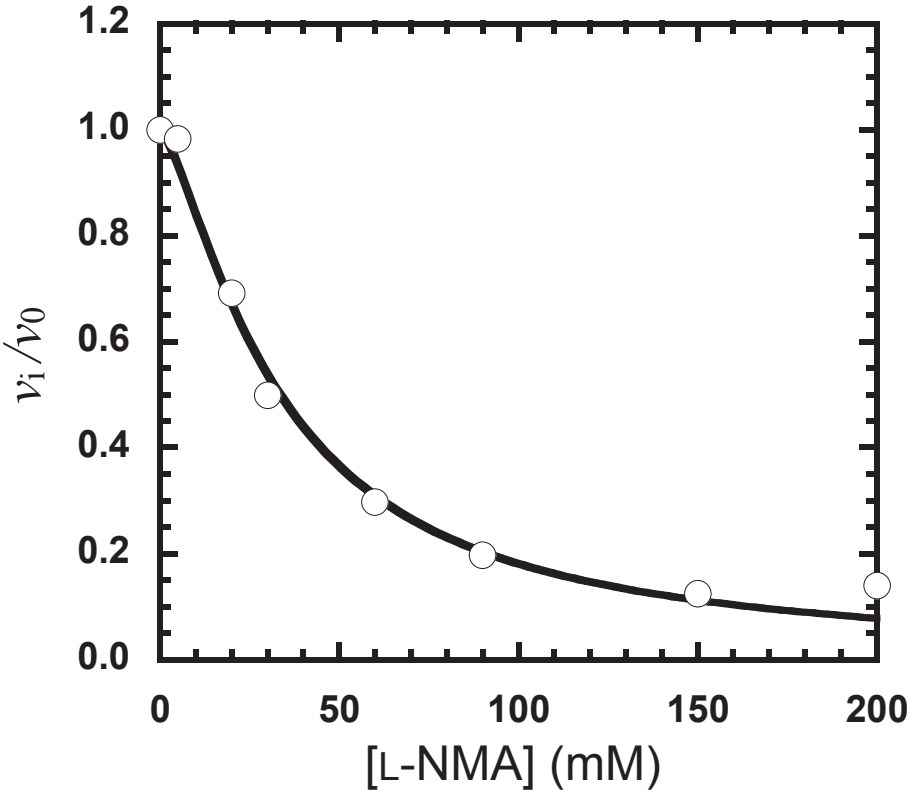

Figure 4.5 Representative IC_{50} curve of *Cs*PR catalysis with L-NMA as the inhibitor. The IC_{50} value was 32.3 ± 1.2 mM and n = 1.4 ± 0.1.

Michaelis constant (K_m >> 250 mM) was much higher than the observed IC_{50} value. To investigate this further, inhibition studies were conducted with L-NMA as an inhibitor for *Cs*PR-catalysed racemisation of L-proline to determine the mode of inhibition. The double reciprocal plot obtained using the initial rates data from these inhibition studies (**Figure 4.6**) suggested that a linear-mixed mode of inhibition is followed by L-NMA, wherein the inhibitor can bind to both the free enzyme and the enzyme-substrate complex. This suggests that L-NMA may bind at an allosteric site. Thus, two binding constants: K_i = 18.5 ± 1.3 mM and αK_i = 47.3 ± 2.5 mM, were determined, resulting in an α value of 2.6 ± 0.2.

4.3.4 L-Azetidine-2-carboxylic acid as a substrate of *Cs*PR

The initial velocities for the *Cs*PR-catalysed racemisation of the four-membered ring analogue of L-proline, L-ACA, obeyed Michaelis-Menten kinetics (**Figure 4.8**). The kinetic constants for the racemisation of L-ACA were K_m = 26.0 ± 0.9 mM and k_{cat} = 22.8 ± 0.6 s^{-1}, showing a ~2.4-fold decrease in the affinity of this alternative substrate compared to L-proline (K_m = 9.5 ± 0.5 mM). The efficiencies of racemisation (k_{cat}/K_m) of L-ACA (0.879 ± 0.005 $mM^{-1}s^{-1}$) and L-proline (8.2 ± 0.1 $mM^{-1}s^{-1}$) catalysed by *Cs*PR showed a ~10-fold difference. Though *Cs*PR has a lower affinity for L-ACA relative to L-proline, *Cs*PR does bind L-ACA better than it binds pipecolic acid, NMA, and NEA (**Table 4.1**).

4.4 DISCUSSION

*Cs*PR-catalysed racemisation of L-NEA showed a much lower catalytic efficiency relative to that of L-proline. To investigate if steric effects were the source for this decrease in efficiency, three other compounds were tested as substrates for *Cs*PR.

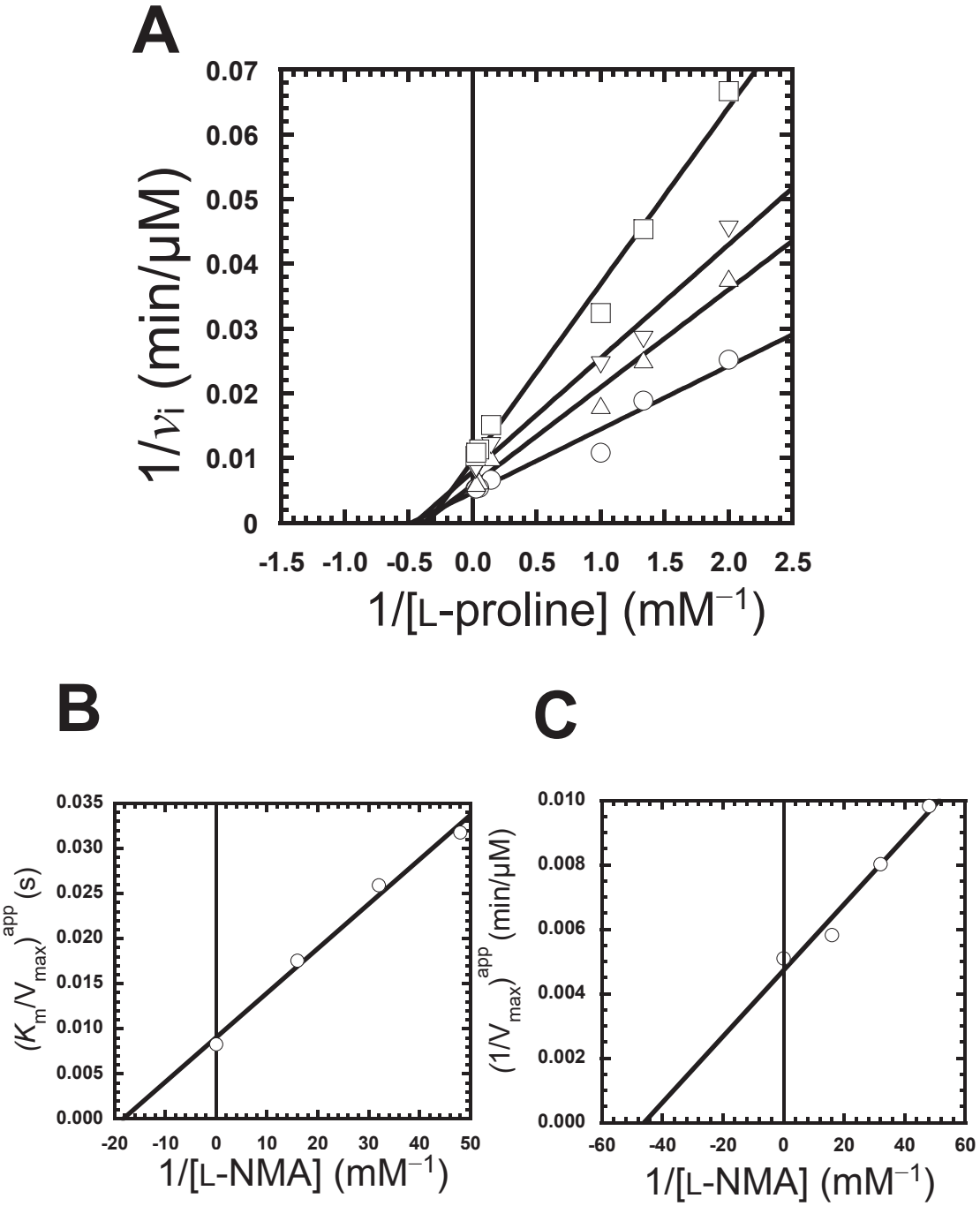

Figure 4.6 Inhibition kinetics of *Cs*PR by L-NMA. (**A**) A representative Lineweaver-Burk plot showing linear-mixed type of inhibition of *Cs*PR by L-NMA. Assays were conducted as described in **section 4.2.5** with the concentration of L-proline ranging between 0.5 and 200 mM, and concentrations of L-NMA equal to 0 mM (○), 16 mM (△), 32 mM (▽), and 48 mM (□). (**B**) A representative replot of apparent K_m/V_{max} values (**B**) and apparent $1/V_{max}$ values (**C**) as a function of the concentration of L-NMA are shown. The negative value of the x-intercepts of the corresponding replots **A** and **B** yield average values of K_i = 18.5 ± 0.4 mM and αK_i = 47.3 ± 0.9 mM, respectively.

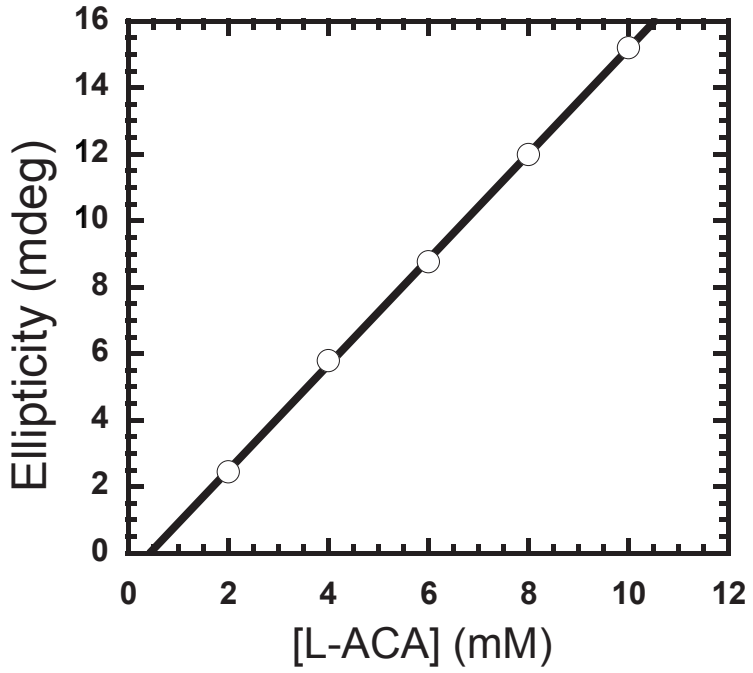

Figure 4.7 Standard curve for the determination of the molar ellipticity of L-ACA. The ellipticities (θ) at 216 nm were determined from the CD spectra. The molar ellipticity ($[\theta]_{216}$) was calculated from the slope of the regression line: $\theta = 1.53689\ (\pm 0.00701)[\text{L-NEA}] + 0.31927\ (\pm 0.00192)$. All experiments were conducted at 15 °C.

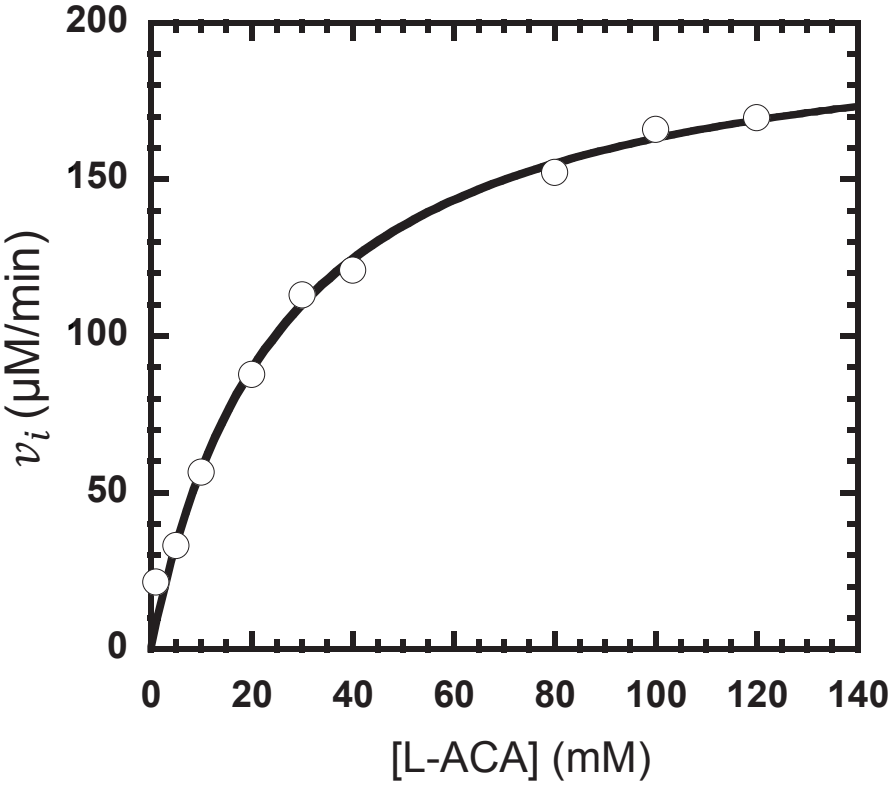

Figure 4.8 Representative Michaelis-Menten plot for *Cs*PR-catalysed racemisation of L-ACA. The values of k_{cat} and K_m are 22.8 ± 0.6 s^{-1} and 26.0 ± 0.9 mM, respectively.

Table 4.1 Summary of the catalytic efficiencies (k_{cat}/K_m) and free energies of activation ($\Delta G^{\ddagger}$) for the racemisation of various substrates catalysed by *Cs*PR.

Substrate	k_{cat}/K_m ($mM^{-1}s^{-1}$)	$\frac{(k_{cat}/K_m)^{substrate}}{(k_{cat}/K_m)^{D/L-pro}}$	$\Delta G^{\ddagger}$ (kcal/mol)	$\frac{(\Delta G^{\ddagger})^{substrate}}{(\Delta G^{\ddagger})^{D/L-pro}}$
L- proline	8.2 ± 0.1	1	11.668 ± 0.007	1
D- proline	14.4 ± 0.1	1	11.346 ± 0.004	1
L- pipecolic acid	0.067 ± 0.005	8.2×10^{-3}	14.42 ± 0.04	1.2
D- pipecolic acid	0.073 ± 0.003	5.1×10^{-3}	14.36 ± 0.02	1.3
L- NEA	0.0018	2.2×10^{-4}	17.8	1.5
L- NMA	0.088 ± 0.006	1.1×10^{-2}	14.26 ± 0.01	1.2
D- NMA	0.058 ± 0.002	4.03×10^{-3}	14.50 ± 0.05	1.3
L-ACA	0.879 ± 0.005	1.1×10^{-1}	12.873 ± 0.003	1.1

All free energy values were calculated at 15 °C.

The results from the study with pipecolic acid, which contains the larger six-membered ring, indicated that pipecolic acid is a substrate of *Cs*PR. The catalytic efficiencies of the racemisation of L-pipecolic acid and D-pipecolic acid were similar, giving a K_{eq} value of 0.92 ± 0.08 (in the L→D reaction direction) as determined from the Haldane relation (Segel, 1968). However, the observed catalytic efficiency with pipecolic acid was ~100-fold lower than the catalytic efficiency of the *Cs*PR-catalysed racemisation of proline (**Figure 4.2**). This suggests that the active site of *Cs*PR can accommodate the large pipecolic acid molecule, but with a much lower affinity relative to proline. Of course, this assumes that the reduction in efficiency arises primarily from a steric effect (i.e., increase in K_m) and not a catalytic effect yielding a decreased value of k_{cat}. This assumption is reasonable since saturation kinetics were not observed (K_m >> 250 mM) as they were when proline was the substrate.

The study with the smaller NMA indicated that *Cs*PR binds NMA and that NMA is a substrate. The catalytic efficiency of the *Cs*PR-catalysed racemisation of L-NMA and D-NMA showed slight variation in their catalytic efficiencies giving a value of K_{eq} equal to 1.5 ± 0.1%, in the L- to D-NMA reaction direction. Interestingly, only a ~10-fold decrease in catalytic efficiency of the *Cs*PR-catalysed racemisation of NMA was observed relative to that of proline racemisation. This suggests that the smaller NMA, where the slight reduction in entropy accompanying replacement of the ethyl group of NEA by the methyl group, results in *Cs*PR binding NEA better than NMA, but still with a lower affinity (K_m >> 250 mM, **Figure 4.5**) relative to proline (K_m = 8.2 mM). Again, that this effect is primarily due to differences in binding is suggested by the observation that NEA and pipecolic acid were turned over by *Cs*PR with similar catalytic efficiencies.

An interesting observation was that the K_m value for the *Cs*PR-catalysed racemisation of NMA is higher than the IC_{50} value of 33.5 mM (**Figure 4.4**) for the inhibition of *Cs*PR by NMA. *Cs*PR seemed to have different affinities for NMA depending on whether NMA was employed as a substrate or as an inhibitor. Further inhibition studies led to the conclusion that NMA inhibited *Cs*PR catalysis by a linear-mixed mode of inhibition (**Scheme 4.1, Figure 4.6**), suggesting that NMA could bind to both the free enzyme (K_i = 18.5 mM) and the enzyme-substrate complex (αK_i = 47.3 mM, α = 2.6). When NMA is used as the inhibitor of the *Cs*PR-catalysed racemisation of proline, the observed change in ellipticity arises from both the turnover of proline and the turnover of NMA by *Cs*PR. Although, the total change in ellipticity ($d\theta_{total}/dt$) can be expressed as the sum of the rates of change in ellipticity due to proline racemisation ($d\theta_{proline}/dt$) and NMA racemisation ($d\theta_{NMA}/dt$) (**equation 4.5**), the latter is essentially negligible based on our substrate turnover studies.

$$\frac{d\theta_{total}}{dt} = \frac{d\theta_{proline}}{dt} + \frac{d\theta_{NMA}}{dt} \tag{4.5}$$

Thus, the total rate of change in ellipticity arises primarily from the ($d\theta_{proline}/dt$) term.

The study with the four-membered ring analogue of L-proline, L-ACA, indicated that L-ACA is a substrate of *Cs*PR, but with a Michaelis constant (K_m) ~3-fold greater than that of L-proline (**Figure 4.8**). L-ACA is a better substrate than pipecolic acid likely due to its smaller size. Interestingly, L-ACA is also a better substrate than NMA, the latter being an analogue of L-ACA with the ring "broken" not unlike the relationship between NEA and proline. Assuming that steric

Scheme 4.1 Reaction mechanism for linear-mixed mode of inhibition of *Cs*PR (E)-catalysed racemisation of L-proline (S) by L-NMA (I)

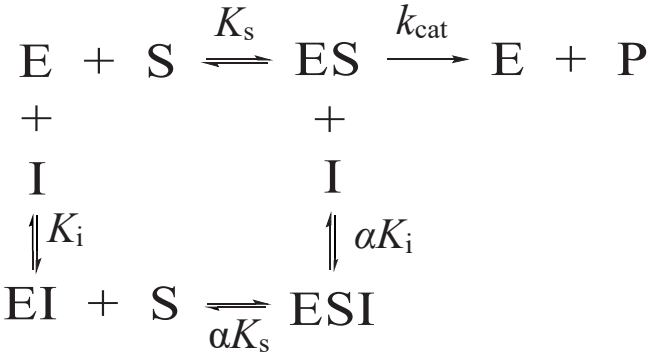

contributions are less pronounced for this system, it would appear that the higher entropic contributions from the methyl group in NMA, disfavours NMA as a substrate with an increase in the free energy of activation of 1.4 kcal/mol relative to L-ACA (**Figure 4.9**).

The ratio of binding constants of L-proline (K_s^{Pro}) and NEA (K_s^{NEA}) can be related to the difference in the corresponding entropies of the substrates as zwitterions in water at 15 °C (ΔS^{Pro} and ΔS^{NEA}) (calculated using Density functional theory-Quantum Mechanics (DFT-QM) calculations at 631-G* level using Spartan Software by Wavefunction, Inc., CA, USA; Bearne, unpublished, **Table 4.2**) by **equation 4.5**, assuming that the difference in their affinities for *Cs*PR arises only from entropic contributions. Similarly, the ratio of binding constants of L-ACA (K_s^{ACA}) and NMA (K_s^{NMA}) and their corresponding entropies in water (ΔS^{ACA} and ΔS^{NMA}) can be related by **equation 4.6**, where R is the gas constant.

$$\frac{K_S^{Pro}}{K_S^{NEA}} = e^{\left(\frac{\Delta S^{Pro}}{R} - \frac{\Delta S^{NEA}}{R}\right)} \tag{4.5}$$

$$\frac{K_S^{ACA}}{K_S^{NMA}} = e^{\left(\frac{\Delta S^{ACA}}{R} - \frac{\Delta S^{NMA}}{R}\right)} \tag{4.6}$$

If an entropic effect is the only factor accounting for the difference in affinities of *Cs*PR towards the substrates, the ratios of their corresponding binding constants [K_s^{Pro}/K_s^{NEA} and K_s^{ACA}/K_s^{NMA}] are expected to be similar. On the contrary, the observed K_s^{Pro}/K_s^{NEA} value <<0.048 and the observed K_s^{ACA}/K_s^{NMA} value <<0.10 (keeping in mind that K_s^{NEA} >>200 mM, K_s^{NMA} >>250 mM, K_s^{ACA} = 26.0 ± 0.9 mM and K_s^{Pro} = 9.5 ± 0.5 mM) which are less than the theoretical values of K_s^{Pro}/K_s^{NEA} (0.042) and K_s^{ACA}/K_s^{NMA} (0.084), calculated by DFT-QM methods and only considering entropy effects. Though entropic contributions affect *Cs*PR catalysis to a

certain extent, steric effects are more pronounced and are likely the primary reason for the loss in catalytic efficiency of *Cs*PR-catalysed racemisation of the substrates that are devoid of a compact ring-structure.

L-ACA **L-NMA**

$\Delta G^{\ddagger}$ = 12.873 ± 0.003 kcal/mol $\Delta G^{\ddagger}$ = 14.26 ± 0.01 kcal/mol

k_{cat}/K_m = 0.879 ± 0.005 $mM^{-1}s^{-1}$ k_{cat}/K_m = 0.088 ± 0.006 $mM^{-1}s^{-1}$

Figure 4.9 A comparison between free energies of activation ($\Delta G^{\ddagger}$) and the catalytic efficiencies (k_{cat}/K_m) of *Cs*PR-catalysed racemisation of L-ACA and L-NMA. The lack of a ring-structure in L-NMA relative to L-ACA resulted in a ~10-fold decrease in catalytic efficiency of *Cs*PR and ~1.4 kcal/mol increase in $\Delta G^{\ddagger}$ values. The $\Delta G^{\ddagger}$ values were calculated at 15 °C.

Table 4.2 Entropies of the substrates as zwitterions in water at 15 °C obtained by DFT-QM calculations at 631-G* level.[a]

Substrate	Entropy in water (J/mol·K)
L-proline	333.97
NEA	360.33
L-ACA	322.09
NMA	342.71

a Bearne, unpublished

CHAPTER 5

CONCLUSIONS

The mesophilic and hyperthermophilic variants of PR examined in this study exhibited very similar free energy profiles with similar contributions of enthalpy and entropy to binding and activation. The crystal structures of PR in the ligand-bound and free enzyme states suggest that the protein undergoes movement from an open state to a closed state such that the bound state forms a highly hydrophobic active site pocket that engulfs the substrate and is not solvent accessible (Buschiazzo *et al.,* 2011). This suggests that although the protein is flexible, the active site of the bound form is less open and only allows for slight movement of the proline side chain. The carboxylate and the protonated amine groups are held in place by multiple hydrogen bonds. A computational study by Rubinstein and Major (2009) suggested that the structure of the PR active site is preorganised in such a way that it limits the movement of proline within the active site. This observation was supported by Harty *et al.*, indicating that the hydrophobic active site of PR is not flexible enough to accommodate bicyclic substrate-product analogue inhibitors (Harty *et al.,* 2014). It is believed that in Nature, an enzyme evolves to the point where the chemical reactions are so fast that the enzyme is limited only by rates of conformational changes or by diffusion (Wolf-Watz *et al.,* 2004). Thus, the lack of significant differences in the free energy of activation ($\Delta G^{\ddagger}$) for the racemisation of proline catalysed by the mesophilic and hyperthermophilic PR variants can be accounted for by the limited flexibility of the PR active site. Hence, both variants have similar free energies of transition state stabilisation of ~ −19 kcal/mol.

L-NEA is a substrate of *Cs*PR but has poor binding affinity to the active site of *Cs*PR relative to proline. Studies with pipecolic acid suggested that sterics effects do impact *Cs*PR catalysis since saturation kinetics were no longer observed (i.e., low binding affinity). However, even though the catalytic efficiency was reduced relative to that observed for proline, the ability of *Cs*PR to catalyse turnover of pipecolic acid indicates that *Cs*PR can accommodate the substrate. The smaller L-ACA is also a substrate of *Cs*PR and the observed kinetic parameters indicate that the catalytic efficiency of L-ACA racemisation, catalysed by *Cs*PR, is greater than for pipecolic acid due to relatively reduced steric effects but less than that of proline. Further, kinetic studies with NMA indicated that L- and D-NMA are both substrates of *Cs*PR and L-NMA is an inhibitor of *Cs*PR catalysis, which suggests that the interaction between NMA and *Cs*PR may be more complex than a simple 1:1 complex - perhaps with the involvement of an allosteric site. The increased affinity of *Cs*PR for the smaller NMA, relative to NEA, can be attributed to the reduction in in size, and perhaps entropy, that arises from the structural differences between them.

These results support the aforementioned constraints in the flexibility of PR active site. The spectrum of substrates of PR studied here have lower affinities for *Cs*PR than proline as the architecture of active site of PR is such that it limits the mobility of the proline ring structure. Thus, pipecolic acid and NEA were bound by *Cs*PR with less affinity than proline due to their increased steric requirements. The less sterically demanding NMA may not bind well because of the increase in entropy accompanying “breaking” of the ring.

If “breaking” the ring leads to a ~10-fold loss in catalytic efficiency of *Cs*PR-catalysed racemisation of L-NMA relative to that of L-ACA, a similar loss might be expected for the catalytic efficiency of *Cs*PR-catalysed racemisation of NEA relative

to that of L-proline. But, we observed a dramatic ~4,500-fold decrease in the catalytic efficiency of *Cs*PR-catalysed racemisation of NEA relative to that of L-proline. This huge loss in catalytic efficiency suggests that, though an intact-ring structure is important for *Cs*PR catalysis, steric effects, in addition to entropic effects, likely are responsible for the major reduction in catalytic efficiency.

When crystals of PR from *T. cruzi* were grown at lower concentrations of PYC (0.1 M), only a single active site of the dimer was occupied. In addition, isothermal titration studies revealed that the two active sites interacted with each other during PYC binding (Buschiazzo *et al.*, 2006). These observations suggest that L-NMA may bind at one active site while the substrate is bound at the other active site of the dimer. Possible, such a binding arrangement could account for the observed linear mixed-type of *Cs*PR by L-NMA.

REFERENCES

Adams, E., and Norton, I. L. (1964) Purification and properties of inducible hydroxyproline 2-epimerase from pseudomonas. *J. Biol. Chem.* **239**, 1525-1535.

Amyes, T. L., and Richard, J. P. (2013) Specificity in transition state binding: the Pauling model revisited. *Biochemistry* **52**, 2021-2035.

Beadle, B. M., Baase, W. A., Wilson, D. B., Gilkes, N. R., and Shoichet, B. K. (1999) Comparing the thermodynamic stabilities of a related thermophilic and mesophilic enzyme. *Biochemistry* **38**, 2570-2576.

Bearne, S. L., and Wolfenden, R. (1995) Glutamate gamma-semialdehyde as a natural transition state analogue inhibitor of *Escherichia coli* glucosamine-6-phosphate synthase. *Biochemistry* **34**, 11515-11520.

Bearne, S.L., and Wolfenden, R. (1997) Mandelate racemase in pieces: effective concentrations of enzyme functional groups in the transition state. *Biochemistry* **36**, 1646-1656.

Bender, M. L., Kezdy, F. J., and Gunter, C. R. (1964) The Anatomy of an enzymatic catalysis. α-chymotrypsin. *J. Am. Chem. Soc.* **86**, 3714-3721.

Buschiazzo, A., Goytia, M., Schaeffer, F., Degrave, W., Shepard, W., Gregoire, C., Chamond, N., Cosson, A., Berneman, A., Coatnoan, N., and Minoprio, P. (2006) Crystal structure, catalytic mechanism, and mitogenic properties of *Trypanosoma cruzi* proline racemase. *Proc. Natl. Acad. Sci. USA* **103**, 1705-1710.

Cardinale, G. J., and Abeles, R. H. (1968) Purification and mechanism of action of proline racemase. *Biochemistry* **7**, 3970-3978.

Conti, P., Tamborini, L., Pinto, A., Blondel, A., Minoprio, P., Mozzarelli, A., and De Micheli, C. (2011) Drug Discovery targeting amino acid racemases. *Chem. Rev.* **111**, 6919-6946.

D'Amico, S., Marx, J. C., Gerday, C., Feller, G. (2003) Activity-stability relationships in extremophilic enzymes. *J. Biol. Chem.* **278**, 7891-7896.

Eyring, H. (1935) The Activated Complex in Chemical Reactions. *J. Chem. Phys.* **3**, 107-115.

Fisher, L. M., Albery, W. J., and Knowles, J. R. (1986) Energetics of Proline Racemase : Racemization of Unlabeled Proline in the Unsaturated , Saturated , and Oversaturated Regimes. *Biochemistry* **25**, 2529-2537.

Gasteiger, E., Hoogland, C., Gattiker, A., Duvaud, S., Wilkins, M. R., Appel, R. D., and Bairoch, A. (2005) Protein identification and analysis tools on the ExPASy server, *The Proteomics Protocols Handbook* (Walker, J. M., Ed.), Humana Press, 571-607.

Harty, M., Nagar, M., Atkinson, L., LeGay, C. M., Derksen, D. J., and Bearne, S. L. (2014) Inhibition of serine and proline racemases by substrate-product analogues. *Bioorg. & Med. Chem. Lett.* **24**, 390-393.

Jaenicke, R., Schurig, H., Beaucamp, N., Ostendorp, R. (1996) Structure and stability of hyperstable proteins: glycolytic enzymes from hyperthermophilic bacterium *Thermotoga maritima*. *Adv. Prot. Chem*. **48**, 181-269.

Jencks, W. P. (1969) *Catalysis in Chemistry and Enzymology,* McGraw-Hill, New York

Kati, W. M., and Wolfenden, R. (1989) Major enhancement of the affinity of an enzyme for a transition-state analog by a single hydroxyl group *Science* **243**, 1591-1593.

Kazemi, M., Himo, F., and Åqvist, J. (2016) Enzyme catalysis by entropy without Circe effect. *Proc. Natl. Acad. Sci. USA* **113**, 2406-2411.

Keenan, M. V., and Alworth, W. L. (1974) The inhibition of proline racemase by a transition state analogue: delta-1-pyrroline-2-carboxylate. *Biochem. Biophys. Res. Commun.* **57**, 500-504.

Koshland, D. E. (1962) The comparison of non-enzymic and enzymic reaction velocities. *J. Theor. Biol.* **2**, 75-86

Kumar, S., Ma, B., Tsai, C. J., Sinha, N., and Nussinov, R. (2000) *Protein Sci*. **9**, 10-19.

Kurihara, S., Oda, S., Kumagai, H., and Suzuki, H. (2006) Gamma-glutamyl-gamma-aminobutyrate hydrolase in the putrescine utilization pathway of *Escherichia coli* K-12. *FEMS Microbiol. Lett*. **256**, 318-23.

Kurihara, S., Oda, S., Kato, K., Kim, H. G., Koyanagi, T., Kumagai, H. and Suzuki, H. (2005) A novel putrescine utilization pathway involves gamma-glutamylated intermediates of *Escherichia coli* K-12. *J. Biol. Chem*. **280**, 4602-4608.

Lienhard, G. E. (1973) Enzymatic catalysis and transition-state theory. *Science* **180**, 149-154.

Lietzan, A. D., Nagar, M., Pellmann, E. A., Bourque, J. R., Bearne, S. L., and Maurice, M. (2012) Structure of mandelate racemase with bound intermediate analogues benzohydroxamate and cupferron. *Biochemistry* **51**, 1160-1170.

Low, P. S., Bada, J. L., and Somero, G. N. (1973) Temperature adaptation of enzymes: roles of the free energy, the enthalpy, and the entropy of activation. *Proc. Natl. Acad. Sci.* **70(2)**, 430-432.

Michael, I. P., and William, P. J. (1971) Entropic contributions to rate accelerations in enzymic and intramolecular reactions and the chelate effect. *Proc. Natl. Acad. Sci.* **68(8),** 1678-1683.

Michaelis, L., and Menten, M. L. (1913) Kinetik der Invertinwirkung. *Biochem. Zeitung* **49**, 333-369.

O'Neal, H. E., and Benson, S. W. (1970) A thermochemical and kinetic analysis of the mechanisms of pyrolysis of polycyclic molecules. *Int. J. Chem. Kinet.* **2**, 423-456.

Page, M. I., and Jencks, W. P. (1971) Entropic contributions to rate accelerations in enzymic and intramolecular reactions and the chelate effect. *Proc. Natl. Acad. Sci. USA* **68**, 1678-1683.

Pal, M., Khanal, M., Marko, R., Thirumalairajana, S., and Bearne, S. L. (2016) Rational design and synthesis of substrate-product analogue inhibitors of α-methylacyl-coenzyme A racemase from *Mycobacterium tuberculosis*. *Chem. Commun.* **13**, 2740-2743.

Pauling, L. (1948) Nature of forces between large molecules of biological interest. *Nature* **161**, 707-709.

Pillai, B., Cherney, M. M., Diaper, C. M., Sutherland, A. S., Vederas, J. C., and James, M. N. G. (2006) Structural insights into stereochemical inversion by diaminopimelate epimerase: An antibacterial drug target. *Proc. Natl. Acad. Sci.* **103**, 8668-8673.

Radzicka, A., and Wolfenden, R. (1995) A proficient enzyme. *Science* **267**, 90-93.

Reina-San-Martín, B., Degrave, W., Rougeot, C., Cosson, A., Chamond, N., Cordeiro-da-Silva, A., Arala-Chaves, M., Coutinho, A., and Minoprio, P. (2000) *Nat. Med.* **6**, 890-897.

Richard, J. P., Amyes, T. L., Crugeiras, J., and Rios, A. (2009) Pyridoxal 5′-phosphate: electrophilic catalyst extraordinaire. *Curr. Opi. Chem. Biol.* **13**, 475-483

Rose, I. A. (1966) Mechanisms of enzyme action. *Annu. Rev. Biochem.* **35**, 23-56.

Rubinstein, A., and Major, D. T. (2009) Catalyzing racemizations in the absence of a cofactor : The reaction mechanism in proline racemase. *J. Am. Chem. Soc.* **131**, 8513-8521.

Rudnick, G., and Abeles, R. H. (1975) Reaction mechanism and structure of the active site. *Biochemistry* **14**, 4515-4522.

Santos, C. R., Tonoli, C. C. C., Trindade, D. M., Betzel, C., Takata, H., Kuriki, T., Kanai, T., Imanaka, T., Arni, R. K., and Murakami, M. T. (2011) Structural basis for branching-enzyme activity of glycoside hydrolase family 57: Structure and stability studies of a novel branching enzyme from the hyperthermophilic archaeon *Thermococcus Kodakaraensis* KOD1. *Proteins* **79**, 547-557.

Schramm, V. L. (1998) Enzymatic transition states and transition state analogue design. *Annu. Rev. Biochem.* **67**, 693-720.

Segel, I. H. (1975) *Enzyme Kinetics*, John Wiley & Sons, Inc., New York.

Siddiqi, F., Bourque, J. R., Jiang, H., Gardner, M., Maurice, M., Blouin, C., and Bearne, S. L. (2005) Perturbing the hydrophobic pocket of mandelate racemase to probe phenyl motion during catalysis. *Biochemistry* **44**, 9013-9021.

Snider, M. J., Gaunitz, S., Ridgway, C., Short, S. A., and Wolfenden, R. (2000). Temperature effects on the catalytic efficiency, rate enhancement, and transition state affinity of cytidine deaminase, and the thermodynamic consequences for catalysis of removing a substrate "anchor." *Biochemistry* **39**, 9746-9753.

St. Maurice, M., and Bearne, S. L. (2004) Hydrophobic Nature of the Active Site of Mandelate Racemase. *Biochem.* **43**, 2524-2532.

Stadtman, T. C., and Elliott, P. (1957) Studies on the enzymic reduction of amino acids. II. Purification and properties of D-proline reductase and a proline racemase from *Clostridium sticklandii*. *J. Biol. Chem.* **228**, 983-997.

Stodulski, M., Jaźwiński, J., and Mlynarski, J. (2008) Synthesis of Yb Complexes with Amino-Acid-Armed Ligands for Direct Asymmetric Tandem Aldol Reduction Reactions. *Eur. J. Org. Chem.* **33**, 5553-5562.

Sundaram, T. K., Wright, I. P., and Wilkinson, A. E. Malate dehydrogenase from thermophilic and mesophilic bacteria. Molecular size, subunit structure, amino acid composition, immunochemical homology, and catalytic activity. *Biochemistry* **19**, 2017-2022.

Thomas, T. M., and Scopes, R. K. (1998) The effects of temperature on the kinetics and stability of mesophilic and thermophilic 3-phosphoglycerate kinases. *Biochem. J.* **330**, 1087-1095.

Tsai, C. J., Ma, B., and Nussinov, R. (1999) *Proc. Natl. Acad. Sci. USA* **96**, 9970-9972.

Vieille, C., and Zeikus, G. J. (2001) Hyperthermophilic enzymes: sources, uses, and molecular mechanisms for thermostability. *Microbiol. Mol. Biol. Rev.* **65**, 1-43.

Villa, J. L., Strajbl, M., Glennon, T. M., Sham, Y. Y., Chu, Z. T., and Warshel, A. (2000) How important are entropic contributions to enzyme catalysis? *Proc. Natl. Acad. Sci. USA* **97**, 11899-11904.

Visser, W. F., Verhoeven-duif, N. M., and Koning, T. J. De. (2012) Identification of a human trans-3-hydroxy-L-proline dehydratase , the first characterized member of a novel family of proline racemase-like enzymes. *J. Biol. Chem.* **287**, 21654-21662.

Watanabe, S., Tanimoto, Y., Nishiwaki, H., and Watanabe, Y. (2015) Identification and characterization of bifunctional proline racemase hydroxyproline epimerase from archaea: discrimination of substrates and molecular evolution. *PLoS One* **10**, e0120349.

Williams, D. H., Stephens, E., and Zhou, M. (2003) Ligand binding energy and catalytic efficiency from improved packing within receptors and enzymes. *J. Mol. Biol.* **329**, 389-399.

Wolfenden, R. (1969) Transition state analogues for enzyme catalysis. *Nature* **223**, 704-705.

Wolfenden, R. (1972) Analogue approaches to the structure of the transition state in enzyme reactions. *Acc. Chem. Res.* **5**, 10-18.

Wolfenden, R. (1976) Transition state analogue inhibitors and enzyme catalysis. *Ann. Rev. Biophys. Bioeng.* **5**, 271-306.

Wolfenden, R. and Snider, M. J. (2001) The depth of chemical time and the power of enzymes as catalysts. *Acc. Chem. Res.* **34**, 938-945.

Wolfenden, R., Snider, M., Ridgway, C., and Miller, B. (1999). The temperature dependence of enzyme rate enhancements. *J. Am. Chem. Soc.* **121**, 7419-7420.

Wolf-Watz, M., Thai, V., Henzler-Wildman, K., Hadjipavlou, G., Eisenmesser, E. Z., and Kern, D. (2004) Linkage between dynamics and catalysis in a thermophilic-mesophilic enzyme pair. *Nat. Struct. Mol. Biol*. **11**, 945-949.